Angular positioning of a door or window

- using a MEMS accelerometer and a magnetometer

Josefin Voigt

LUND UNIVERSITY

verisure

Master's Thesis
Electrical Measurements

Faculty of Engineering, LTH
Department of Biomedical Engineering

Advisor: Johan Nilsson
Co-advisor: Filip Skarp
Co-advisor: Martin Stridh

Acknowledgements

Firstly I would like to thank my supervisor at Verisure Innovation AB in Malmö, Filip Skarp for his great guidance and continuous discussions during the course of this master thesis.

I would also like to thank the rest of the product group at Verisure Innovation for their valuable input and help in the progression of the master thesis.

I would also like to thank my supervisors at LTH, Johan Nilsson and Martin Stridh, for their time and support.

Furthermore I would like to thank the open source community for sharing lots of code online, which has simplified much of this master thesis.

I would also like to thank STMicroelectronics for providing the devices used for testing in this master thesis.

Finally I would like to thank my family and friends for continuous support and interest in this master thesis work.

Abstract

The accurate and reliable detection of opening of doors and windows is vital for home security applications. This master thesis aims to present a way to achieve this using a low-cost and low-power e-compass, containing a MEMS accelerometer and a magnetometer.

This has been achieved by attaching such a device to a door and collecting sensor data when opening and closing the door. Said data were then analysed in the Matlab environment to study the impact of different methods found in literature to correct for errors in measurements. These include Zero Velocity Compensation for the accelerometer values and hard- and soft-iron compensation for the magnetometer. Thereafter the angle of opening has been calculated, using corrected measurement values.

The finished algorithm has also been adapted for implementation on a Cortex-M4 CPU as this, or a similar processor, is likely what is available to use with the e-compass in a real world application. This also motivates the adjustment of the algorithm to use less memory.

Finally said implementation has been performed.

The results show that it is possible to correct for most of the errors of the accelerometer, but the errors that are left will still propagate to the angular calculations, causing the angle to drift. This can be compensated for by using the angle calculated from magnetometer measurements. The correction of effects affecting the magnetometer is also mostly successful.

Likewise the implementation of the algorithm on the processor shows promising results. However, to generalise the algorithm to work on all kinds of doors, as opposed to only the doors it has been developed on, further studies are required.

Sammanfattning

För alla typer av inbrottsskydd är det viktigt att detektera om ett fönster eller en dörr öppnas, då detta kan vara ett tecken på inbrott. För sagda detektion används idag en magnetkontakt. Denna komponent har dock ett antal nackdelar, däribland möjligheten att störa den med en extern magnet. I detta examensarbete har en alternativt metod utvärderats, baserat på en så kallad eKompass (eCompass på engelska), bestående av en accelerometer och en magnetometer.

Detta har uppnåtts genom att fixera en sådan komponent på kanten av en dörr och samla mätdata då dörren öppnas och stängs. Den uppmätta datan har sedan analyserats i Matlab för att studera olika publicerade metoders förmåga att korrigera för mätfel. Dessa metoder innefattar bland annat så kallad Zero Velocity Compensation (Nollhastighets-kompensering) av accelerometerdatan samt kompensering av hård-och mjuk-järnseffekter av magnetometerdatan. Vinkeln har därefter beräknats utgående från de korrigerade mätvärdena.

Den slutliga algoritmen har även implementerats på en Cortex M4 CPU då denna, eller en liknande processor, troligtvis är vad som finns tillgängligt för användande med en eKompass i en verklig applikation. Detta är också motivationen för den lågminnes-anpassning som gjorts i detta arbete.

Resultaten visar att det är möjligt att korrigera för majoriteten av de fel som påverkar accelerometern, men de resterande felen kommer att propagera till beräkningarna av vinkeln. Detta kommer orsaka drift in vinkelberäkningarna, vilket i sin tur kan kompenseras med hjälp av beräkningar av vinkeln baserat på magnetometerdata. Korrigeringen av magnetometerdatan är mestadels framgångsrik.

Även implementationen av algoritmen på processorn uppvisar lovande resultat. För att generalisera algoritmen så att den fungerar på alla sorters dörrar och inte bara de dörrar den utvecklats på behövs mer arbete.

Glossary

Cortex-M4 processor A high performance embedded processor, p. 5

g unit of measurement for acceleration, equal to 9.82 $\frac{m}{s^2}$, p. 10

Hard-iron effects Permanent magnetic fields on the PCB affecting the magnetometer measurements, p. 17

LSM303DLHC An e-compass from STMicroelectronics featuring an accelerometer and a magnetometer, p. 4

pitch θ, rotation around the y-axis, p. 23

roll ϕ, rotation around the x-axis, p. 23

Soft-iron effects Magnetic fields in the environment inducing varying magnetic fields on the PCB, influencing the magnetometer measurements, p. 18

STM32F3 Discovery A development kit from STMicroelectronics featuring an e-compass, p. 4

STM32F401C Discovery A development kit from STMicroelectronics featuring an e-compass, p. 5

yaw ψ, rotation around the z-axis, p. 24

Acronyms

BNEA Brownian Noise Equivalent Acceleration - Thermo-mechanical noise of the accelerometer, p. 10

DWT Discrete Wavelet Transform - A wavelet transform using discretely sampled values, p. 39

IMU Inertial Measurement Unit - Component that consists of accelerometer, magnetometer and gyroscope, p. 7

MEMS Microelectro-Mechanical Systems - Systems on the micrometer scale, fabricated using special techniques, p. 1

ODR Output Data Rate - Rate at which data is sent from a component, p. 32

PCB Printed circuit board - Circuit board connecting the component and processors, p. 18

ZVC Zero Velocity Compensation - Method to compensate for errors arising from integration of acceleration, p. 41

Contents

1 Introduction **1**
- 1.1 Motivation . . . 1
- 1.2 Goals . . . 1
- 1.3 Adaptation . . . 2

2 Measurement setup **3**

3 Components **7**
- 3.1 Accelerometer . . . 7
  - 3.1.1 Basic operating principles of the capacitive accelerometer . . . 7
  - 3.1.2 Accelerometer error and noise sources . . . 10
  - 3.1.3 Expected measurement values . . . 11
- 3.2 Magnetometer . . . 14
  - 3.2.1 Basic operating principles . . . 15
  - 3.2.2 Magnetometer error sources . . . 16
  - 3.2.3 Expected measurement values . . . 19
- 3.3 Gyroscope . . . 22

4 Frame of reference **23**
- 4.1 Description . . . 23
- 4.2 Finding the rotation . . . 25
- 4.3 Derotating the measurement values . . . 27
  - 4.3.1 Derotating to find the magnetometer angle . . . 28

5 Algorithm **30**
- 5.1 Calibration . . . 32
  - 5.1.1 Finding hard-iron offsets . . . 33
  - 5.1.2 Finding soft-iron effects and scale-factors . . . 34
  - 5.1.3 Finding accelerometer scale-factors and offsets . 35
  - 5.1.4 Finding yaw-scaling . . . 36
- 5.2 Filtering . . . 37
  - 5.2.1 Moving average filtering . . . 37

5.2.2 Frequency filtering . . . 38
5.2.3 Wavelet filtering . . . 39
5.3 Zero Velocity Compensation . . . 40
5.3.1 Description . . . 41
5.3.2 Implementation for the movement of a door . . . 42
5.3.3 Detecting movement . . . 43
5.4 Connecting the component measurements . . . 44
5.4.1 Accelerometer alone . . . 44
5.4.2 Correction using the magnet contact . . . 44
5.4.3 Correction using the magnetometer . . . 45
5.5 Adaptation to implementation on a processor with limited memory . . . 46
5.5.1 Compensating the ZVC . . . 46
5.5.2 Avoidance of memory storage . . . 47
5.5.3 Finding hard and soft-iron effects . . . 47
5.5.4 Sampling rates . . . 47
5.6 Detection of tampering . . . 48
5.7 Window opening in the plane of gravity . . . 50

6 Results **52**
6.1 Accelerometer . . . 52
6.1.1 Raw data . . . 52
6.1.2 Filtering . . . 54
6.1.3 Correcting rotation . . . 59
6.1.4 ZVC . . . 62
6.1.5 Adaptation of sampling rate for power savings . 65
6.2 Magnetometer . . . 68
6.2.1 Raw data . . . 68
6.2.2 Correcting rotation . . . 69
6.2.3 Correcting for hard- and soft-iron effects . . . 70
6.2.4 Adaptation of the calibration for low power operation . . . 76
6.2.5 Yaw-scaling . . . 80
6.3 Components together . . . 81
6.3.1 Correction without other signals . . . 81
6.3.2 Correction using magnet contact . . . 81
6.3.3 Correction using the magnetometer . . . 83
6.4 Implementation on Cortex-M4 processor architecture . 86
6.5 Window opening in the plane of gravity . . . 87

7 Discussion **89**

8 Conclusion **92**

Appendices **93**

A Finding hard- and soft-iron effects **94**

B Implementing the algorithm in C-code **98**

C Effects of algorithm operations on measurement values **100**
C.1 Accelerometer 100
C.2 Magnetometer 103

1. Introduction

1.1 Motivation

In home security of today it is important to be able to determine whether a door or window is open or closed, as an unexpected opening might indicate a break-in. Some sort of sensor to be placed on the door or window is therefore required. Today a magnetic contact is often used. However there are some disadvantages to this component; the fact that an external magnet can disturb it, the need for two components to be installed (one on the door frame and one on the door, in the door case) or the potential risk of misaligning these two components during installation, which would hinder the proper functioning of the magnet contact. Therefore this report aims to investigate an alternative component for the determination of the state of the door or window, open or closed.

This component would need to be very low-power since it is wireless and therefore will be powered with a battery, but still needs to have a life-time in the span of years. Recent development in the MEMS (microelectro-mechanical systems) accelerometers on the market provides just such a sensor; low power but still reacting to movement of the door or window.

To decrease the length of the sentences in the report, the algorithm is developed for doors, but the same principle can be used for windows.

1.2 Goals

The initial goals of this master thesis are therefore to:

- Examine different ways to determine whether the door or window is open or closed based on sensor data from an accelerometer
- Compare different position determining algorithms

- Optimize the best algorithm for a battery-powered component
- Implementation of the best algorithm on Cortex M3 processor architecture as a demonstration

1.3 Adaptation

During the work process it became evident that the accelerometer is not able to deliver information with the reliability necessary for a home safety application. Therefore a magnetometer was included in the measurement setup, as an additional source of information. The first goal has therefore been expanded to:

- Examine different ways to determine whether the door or window is open or closed based on sensor data from an accelerometer and a magnetometer

2. Measurement setup

To be able to determine whether the door is open or closed the usage of certain sensors are required. These are included in different products to be described in this section.

At first the lone acceleration measurements were taken using an accelerometer from Analog Devices, **ADXL362**. This device was included on a development board, see figure 2.1a that was attached to a door as per figure 2.1b. Note that the chord connecting the device to the computer for power supply and logging is not shown. Compatible software was available online from the Analog devices homepage. Said software was used to create text files with the measured accelerations of the opening of different doors at the Verisure office in Malmö. This was then analysed using the Matlab environment.

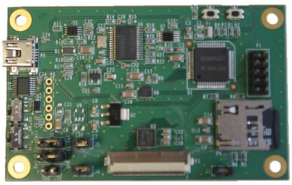

(a)

(b)

Figure 2.1: (a) Close-up of the adxl362 development board used. (b) Device attached to the door for measurements.

As it became apparent that the accelerometer alone was unable to provide angular information with sufficient security another device was studied. The choice fell on the STM32F3 Discovery board from STMicroelectronics. This development board includes, among other things, an e-compass; **LSM303DLHC**. This e-compass consists of an accelerometer and a magnetic sensor, that is a magnetometer. Measurement data from the opening of doors at Verisure using this device was also recorded. The resulting accelerometer and magnetometer values were also analysed in the Matlab environment.

An algorithm was then developed in this environment based on the measurement data as well as theory of operation. To compare the accuracy of the computed angle with a known working device a magnet contact was also attached to the STM32F3 Discovery kit, according to figure 2.2. The signal of open or closed from this device was also registered during measuring.

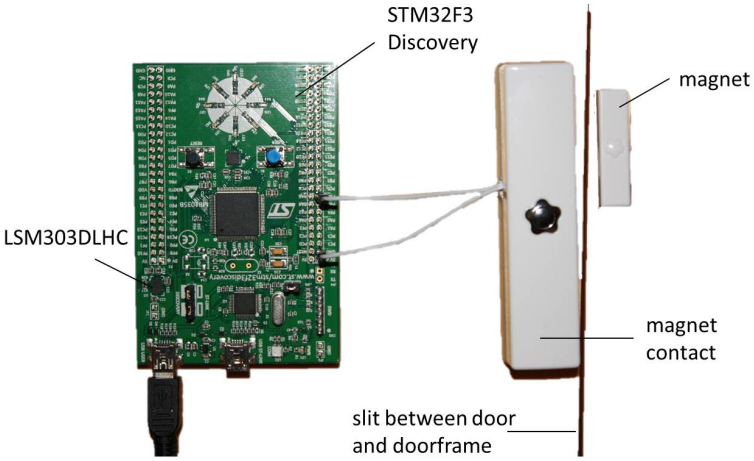

Figure 2.2: The set-up for the STM32F3 Discovery kit, used to take accelerometer and magnetometer values, together with the magnet contact.

The final algorithm was then transformed to c code using the built-in code converter of Matlab. Thereafter the c code was cleaned up to make the operations more effective.

Finally another discovery board from STMicroelectronics, the STM32F401C-

Discovery kit , see figure 2.3, was used to implement the algorithm in real time.

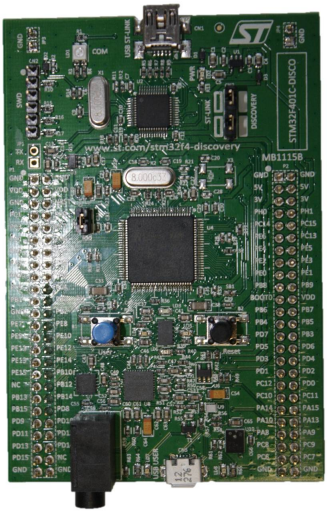

Figure 2.3: The STM32F401 Discovery kit, used to implement the algorithm in real time.

This discovery board features the same e-compass, the LSM303DLHC, as the STM32F3 discovery board. Furthermore this device has an ARM Cortex-M4 CPU (processor) . Even though the goal stated that the implementation should be done on Cortex-M3 processor architecture, since this was available on a development board accessible at the time, Cortex-M4 implementation was deemed to be a good replacement. Using one of the featured development tool-chains, Atollic TrueSTUDIO, and software found on-line at the homepage of STMicroelectronics, the algorithm was then implemented on the STM32F401 Discovery. To illustrate the open and closed state of the door LEDs were used. When the door was opened certain LEDs were lit up and when it was closed others were activated instead.

The magnet contact was attached to this board as well. This finally enabled a USB memory stick connected to the board to log the angular information from the algorithm as well as the data from the magnet

contact. To be able to run the algorithm with the USB memory stick attached the code was further developed in the eclipse environment.

3. Components

To determine heading in for instance aircrafts a so called Inertial Measurement Unit (IMU) is often used [1]. It can also be used in other kinds of position determining applications [2]. This is a component consisting of a magnetometer, accelerometer and a gyroscope, which can give quite a full image of the movement of an object. However in this work only an accelerometer and a magnetometer has been used to determine the angle of the door. The reason for excluding the gyroscope is mainly due to its higher current consumption.

3.1 Accelerometer

An accelerometer is simply a component that senses acceleration. This can be achieved in a number of different ways, where the most common are the displacement accelerometers. These are accelerometers where the sensing elements consist of masses that are displaced due to an external force. They usually work in one of three ways, giving rise to three different kinds of accelerometers; the piezoresistive, the piezoelectric and the capacitive. The advantage of the capacitive version is that it avoids the temperature dependence of piezoresistors [3]. The accelerometer studied in this work is probably a capacitive accelerometer[4], which is the most common form of accelerometers[5].

For this study accelerometers with three axes forming a 3 dimensional coordinate system [6] are used.

3.1.1 Basic operating principles of the capacitive accelerometer

The sensing element in a displacement accelerometer typically consists of a so called proof-mass (basically a lump of conducting material) suspended above a substrate by compliant springs [7], as illustrated in figure 3.1.

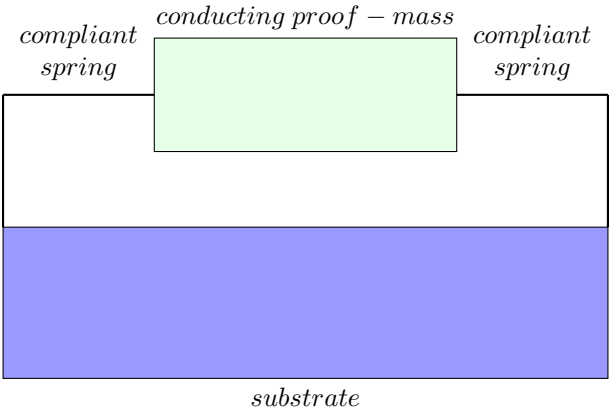

Figure 3.1: Side view of the relation between the proof-mass, substrate and compliant springs in a displacement accelerometer.

When this structure is subjected to a force of some kind the proof-mass is displaced in relation to the substrate, hence the name displacement accelerometer, and the distance d, shown in figure 3.2, is changed. The force mentioned can result from an acceleration according to Newtons second law:

$$F = ma \tag{3.1}$$

where F is the force, m the mass and a the acceleration [8], [9]. The resulting displacement of the proof-mass, Δd can under certain conditions be proportional to the input acceleration

$$\Delta d = \frac{ma}{k} \tag{3.2}$$

where k is the spring constant of suspension [8], [3].

Attached to the surface (without springs) are stationary electrodes, as can be seen in figure 3.2.

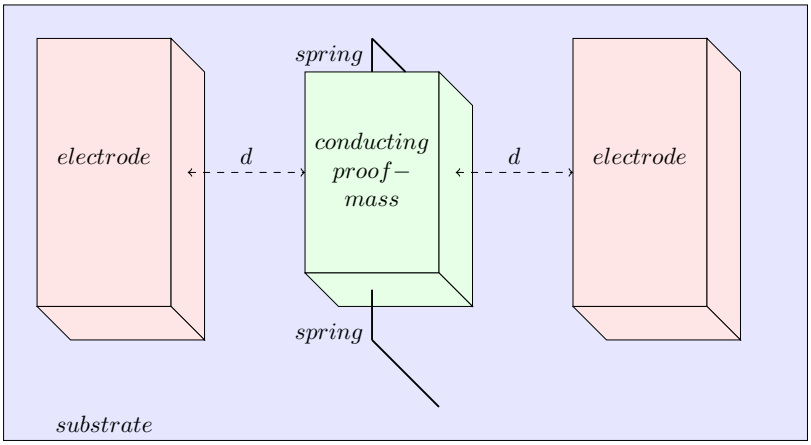

Figure 3.2: Top view of the relation between the proof-mass and the electrodes.

Between these electrodes and the electrically conducting proof-mass two sense capacitors are formed, thus comprising a capacitive half-bridge. As the proof-mass is displaced due to acceleration the distance, d, between the proof-mass and the electrodes are changed, which in turn changes the measured capacitance, as capacitance is related to the distance between the two conducting materials according to the formula [10]:

$$C = \epsilon_r \epsilon_0 \frac{A}{d} \tag{3.3}$$

Here C is the capacitance, ϵ_r the dielectric constant of the material between the electrodes and the proof-mass, ϵ_0 the vacuum permittivity, A the area of overlap of the proof mass and the electrode and finally d is the distance between the electrode and the proof-mass. At the change of d one of the capacitances will increase (the one approached by the proof-mass) and the other decrease (the other). This change in capacitance causes a change in the capacitive half-bridge [7], which can be measured using different techniques.

Furthermore a so called force-balanced accelerometer can be used. In this case the displacement of the proof-mass is counteracted by the application of a feedback force, often in the form of an electro-statical force. The feedback force needed to keep the proof-mass stationary is here measured and gives rise to the output signal [7].

In the components used in this project the conversion between the measured imbalance of the capacitances and the original acceleration is handled by the manufacturer and only the acceleration is output.

3.1.2 Accelerometer error and noise sources

The accelerometer is very good at sensing gravity, since that is one strong force affecting the proof-mass. Therefore one big source of error for the accelerometer can be misalignment of the coordinate system with respect to gravity. This would cause the measurements along the axes supposedly orthogonal to gravity to be in fact affected by gravity. This can be handled by derotating the measured values, using the calculated rotation, as found in section 4.

Another factor resulting in errors in the measurements is a bias error. This means the deviation from 1 g in an axis perfectly aligned with gravity and from 0 g in the axes perfectly perpendicular to gravity. This can occur due to a multitude of reasons, such as mechanical tolerances in the PCB, screws, standoffs and other component parts [11]. Said bias can be measured for instance by simply aligning the accelerometer with gravity and derotating the values to avoid possible misalignment. The deviation from the ideal values can then be stored as an offset to be subtracted from all of the following values. Alternatively it can be decided by averaging two measurements taken at 180 degrees rotational difference from one another.

There are many other error sources that might affect the measurements, such as the temperature dependence (change of output values with temperature) or cross axis sensitivity (acceleration affecting the axes perpendicular to the applied force) to name a few. These will not be further described and the interested is recommended to read further in [11].

A big contributor to the total noise is the thermal noise. Due to the random motion and collisions of molecules within the accelerometer, so called Brownian motion, some agitations occur. This generates basically white noise. The root mean square of this noisy signal is known as the thermal noise equivalent acceleration (TNEA) [8], also known as Brownian noise equivalent acceleration (BNEA)[12] or thermo-mechanical noise [11]. This can be described as

$$BNEA = \sqrt{\frac{4k_B T\omega_0}{MQ}} \tag{3.4}$$

with k_B corresponding to the Boltzmann constant, T the temperature, ω_0 the accelerometer's natural angular frequency, M the mass of the proof-mass and Q the mechanical quality factor.

For the accelerometer used in this report, the one incorporated in LSM303DLHC from STMicroelectronics, the acceleration noise density in normal mode is 220 $\mu g/\sqrt{Hz}$ [13]. To learn the corresponding root-mean-square acceleration noise (BNEA) one simply multiplies the noise density with the square root of the bandwidth and a factor depending on the filter used [11]. For instance, using a 50 Hz first-order lowpass Butterworth filter, with a filter factor of 1.57, the resulting noise would be 1.95 mg. This corresponds to approximately 0.02 $\frac{m}{s^2}$.

3.1.3 Expected measurement values

Since the accelerometer measures forces acting on a proof-mass it will foremost sense gravity. Aside from this it will measure acceleration due to movement, a fact which is utilised in this report.

As the accelerometer is attached to a door its path will be limited to a demi-circle. Circular motion in turn give rise to a centripetal force, F_c, with a radial component F_r always directed towards the centre of the circle, and a tangential component F_T, which is directed tangentially to the circle at a certain point. The acceleration giving rise to these forces can likewise be separated into a tangential, a_T, and a radial part, a_r. This is illustrated in figure 3.3.

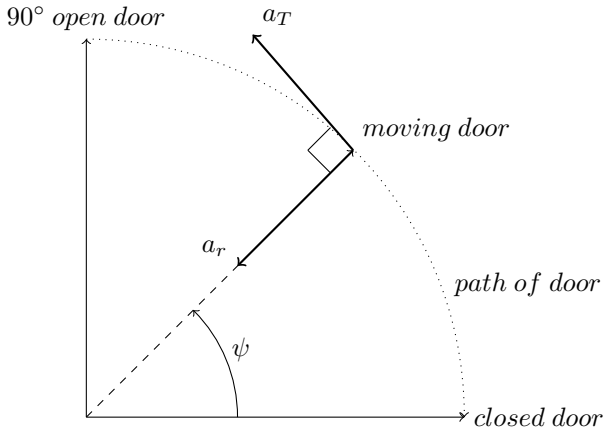

Figure 3.3: Accelerations of the moving door

Since the accelerometer has three measurement axes the objective when attaching the accelerometer to the door is to align one of the axis with the radial acceleration (in the plane of the door) and the other with the tangential acceleration (orthogonal to the plane of the door). Gravity should then be isolated to the last axis, which should be aligned with gravity. Certain misalignment will surely occur, how to compensate for this is described in section 4.

The resulting measured acceleration is related to the angular frequency, ω of the door as follows in eq. (3.5) - (3.6), [9].

$$|a_r| = \omega^2 R \tag{3.5}$$

$$a_T = R\frac{d\omega}{dt} \tag{3.6}$$

where R is the radius of the circle, being the distance from the hinges of the door to the accelerometer, and $\frac{d\omega}{dt}$ the time derivative of the angular frequency, also known as the angular acceleration. In the case of a window the radius can simply be changed accordingly. This gives rise to two different ways of calculating the angular frequency, which in turn permits the calculation of the angle, ψ [9], of the door at a certain moment in time.

$$|\omega_r| = \sqrt{\frac{|a_r|}{R}} \tag{3.7}$$

$$\omega_T = \int (\frac{a_T}{R}) dt \tag{3.8}$$

$$\omega = \omega_r = \omega_T$$

$$\psi = \int \omega dt \tag{3.9}$$

where t is the time. Here both the ways of calculating ω should give the same magnitude of the angular velocity. However since the radial component of the acceleration is always directed in the same direction, no matter which direction the door is moving, the direction of the angular velocity cannot be deduced without looking at the tangential component. During calculations of the angle it is therefore assumed that the direction of the angular velocity for both components is determined by the direction of the tangentially calculated angular velocity.

As can be seen the determination of the angle using the tangential acceleration is dependant on integrating twice. It is a known problem that any error in the initial acceleration will propagate, [14], [15], to cause large displacements of the angle in the final curves.

Since both these ways of determining the angle are dependant on the radius it would be advantageous to find a way of performing these calculations without this dependence. This would namely be another parameter which would need to be provided by the installer, as the radii of doors and windows can vary. One way of achieving this could be to use the following approach.

$$
\begin{aligned}
\frac{a_T}{a_r} &= \frac{R\frac{d\omega}{dt}}{-\omega^2 R} \\
\frac{a_T}{a_r} &= -\frac{d\omega}{dt}\omega^{-2} \\
with\ \ y = \frac{1}{\omega} \ &\Rightarrow\ \ \frac{dy}{dt} = \frac{d\omega}{dt}\omega^{-2} \\
\int \frac{dy}{dt}dt &= -\int \frac{a_T}{a_r}dt \\
y &= C - \int \frac{a_T}{a_r}dt \\
\omega(t) &= \frac{1}{C - \int_0^t \frac{a_T(s)}{a_r(s)}ds}
\end{aligned}
\tag{3.10}
$$

where C is the initial value of y, (when it is different from 0) arising from the fact that we are integrating over a limited time period and the accelerations are integrated from 0 to the current time. However, this formula requires the measured accelerations to be divided by each other, which can be complicated with real measurement values since they will not necessarily go to 0 at the same time. When the denominator then goes to 0 before the nominator due to noise the resulting value would be infinity. If it does work the angle of the door, ψ can be calculated as shown in eq. (3.9).

3.2 Magnetometer

A magnetometer basically measures the magnetic fields in its surroundings, this includes the geomagnetic fields, as well as magnetic fields arising from permanent or temporary magnets, such as ferromagnetic materials.

An ideal magnetometer in an environment far from any permanent magnets or ferromagnetic materials will only measure the geomagnetic field, being the magnetic field of earth.

Magnetometers coupled with accelerometers are often used as so-called eCompasses (electronic compasses), which function as normal compasses (based on magnets), but require a power source, such as a battery, to function.

3.2.1 Basic operating principles

The magnetometer of the device used for this report utilizes so called Anisotropic Magneto-resistive technology (AMR) to determine the value of the magnetic field [16].

The basic idea behind mangetoresistive magnetometers is that an external magnetic field will cause a change in resistance. This is implemented by using a ferromagnetic [16] material such as a permalloy (an alloy of nickel and iron)[17]. When a current passes through such a material it is magnetized in the direction parallel to the current. However, when it is exposed to an external magnetic field, perpendicular to the current, the magnetization of the material will turn towards the new external field, away from the current direction. This in turn causes the resistance of the material to decrease as the electrons moving in the direction of the magnetization have a larger possibility of being scattered [17]. Since the conductive electrons move in the current direction, which is no longer parallel to the magnetization they will scatter less and the resistance will decrease.

The sensor itself consists of four ferromagnetic resistors positioned in a Wheatstone bridge[16], see figure 3.4. The opposite elements in this configuration will have the same polarities, that means R_1 and R_2 will have the same polarization, which is opposite to R_3 and R_4 that have the same polarization. This causes the resistance to change differently in the different elements of the bridge when applying an external magnetic field. This in turn causes a voltage change between node A and B in the Wheatstone bridge, which can be measured. When no magnetic field is applied the voltage difference is 0.

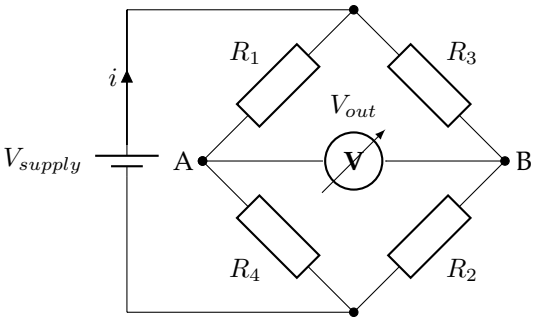

Figure 3.4: Wheatstone bridge used to measure the change in resistance in the magnetoresistive components, R_1 to R_4 due to a change in the magnetic field.

3.2.2 Magnetometer error sources

One possible source of error for the magnetometer is misalignment of the axes in relation to the horizontal and vertical component of the geomagnetic field. To compensate this one can derotate the values, using the rotation as found in section 4.

Furthermore any iron in the environment, common in indoors, can distort the magnetic field [18].

Another, big, cause of magnetometer error is the hard-iron effects and the soft-iron effects. One can envision perfect magnetometer-readings, unaffected by either hard-iron effects or soft-iron effects, only measuring the geomagnetic fields, as a sphere of possible measurement values with centre in the origin and radius equal to the geomagnetic field strength, B, as per figure 3.5.

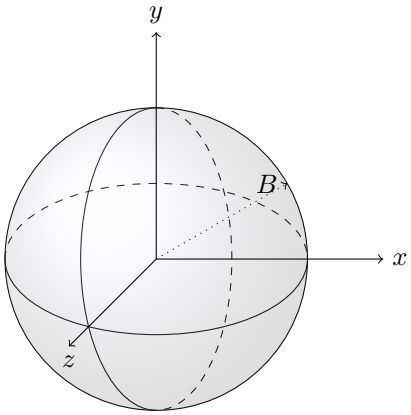

Figure 3.5: Possible perfect magnetometer values without other external magnetic field than the geomagnetic field

When subjected to hard- and soft-iron effects this sphere of possible magnetometer readings will be affected [19]. How to determine the hard-and soft iron effects is described in appendix A.

3.2.2.1 Hard-iron effects

Hard-iron effects are usually generated by permanent magnets or permanently magnetized ferromagnetic materials on the circuit board [20], [21]. This could be for instance audio speakers and buzzers. Also normally demagnetized ferromagnetic materials, such as steel, can be permanently magnetized by the permanent magnetic components in their vicinity. Hence these effects are time-invariant.

Since all these magnetic components and their corresponding magnetic fields are fixed on the circuit board their effect on the sensor will be constant. Thus if you move or turn the circuit board the influence of these effects on the magnetometer readings will remain the same.

Therefore these hard-iron effects can be simply envisioned as an offset in each measurement direction for the magnetometer [19]. The resulting effect on the sphere of possible measurement values can be seen in figure 3.6.

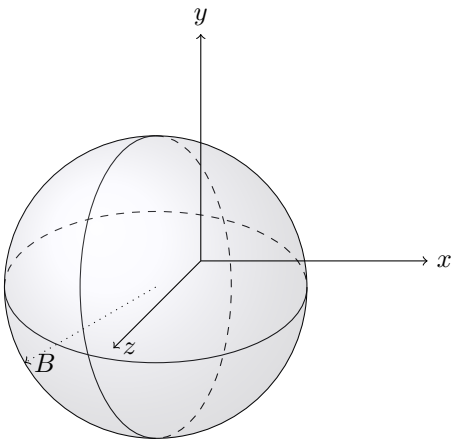

Figure 3.6: Possible magnetometer values distorted by hard-iron effects

Fixed currents on the circuit board generates magnetic fields that will also add to these effects [20].

Since said effects depend on fixed magnetic fields that will not change with time or orientation they can be pre-calibrated before usage and no further measurements are theoretically necessary during usage.

3.2.2.2 Soft-iron effects

Soft-iron effects are normally generated by the geomagnetic field inducing temporary magnetic fields in soft-iron ferromagnetic materials, on the circuit board [20]. Soft-iron magnetic materials are materials that will return to being non-magnetized when the external magnetic field is removed [22]. These soft-iron effects will then vary depending on the rotation of the PCB (printed circuit board) compared to the external magnetic fields (geomagnetic and potentially other surrounding fields). Also current traces on the board can contribute to the generation of this time-varying field [21].

Since the impact of soft-iron effects on the magnetometer measurements depend on the rotation, this means that for certain directions the maximum value of the magnetic field will be much greater than for other directions, even when compensating for hard-iron effects. If one envisions the sphere of possible values the soft-iron effects will transform this sphere into an ellipsoid [19], according to figure 3.7.

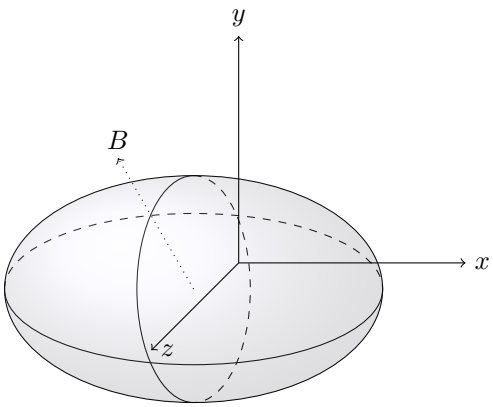

Figure 3.7: Possible magnetic measurement values distorted by hard-iron and soft-iron effects.

In this picture the ellipsoid seems to be aligned with the x-axis, which does not necessarily concur with reality, as it can be aligned in any direction. To express this mathematically the soft-iron effects are usually modelled as a symmetric matrix to be multiplied with the original magnetometer values. Since said effects vary with rotation it is necessary to recalculate the soft iron-effects for every orientation of the magnetometer and a continuous update is required during usage.

Furthermore mismatching of the sensitivities of the different sensing axes of the magnetometer can affect the results [21]. This means that different axes of the magnetometer will not give equal output when exposed to identical magnetic fields. This is called a scale-factor error which will also transform the sphere into an ellipsoid, which makes these factors hard to distinguish from soft-iron effects when simply studying the resulting measurement values.

Since these effects can be time varying they are more complex to correct for in retrospect. They are therefore often removed by other means, such as shielding the magnetometer from the sources of disturbance or simply placing the magnetometer further away from these sources[18].

3.2.3 Expected measurement values

The geomagnetic field, measured by a magnetometer in a disturbance-free environment, varies in intensity, from around 66 μT close to Antarctica to approximately 23 μT around Paraguay [23]. The possible measurement values when turning the magnetometer will therefore be situated on the surface of a sphere, centred in the origin, with the radius corresponding to the absolute value of the measurement, being equal to the geomagnetic field.

The strength of the geomagnetic field can be described as a vector pointing to north. However this vector will not be horizontal, instead it will point partly towards the ground. The angle between the horizon and the geomagnetic field vector is known as the inclination angle, often noted as δ. In Malmö this angle is approximately 70° [23].

This geomagnetic field vector can thus be split into two components, one horizontal field vector perpendicular to gravity and one vertical field vector parallel with gravity.

Since the magnetometer in these applications will be placed on a circuit board with an accelerometer as well as a processor, certain hard-iron effects are expected. These can be modelled as a simple additive vector, V, to the actual magnetic values. Without these effects the sphere of the possible measurement values will be centred in the origin, but the hard iron effects will cause a displacement of the centre of the sphere.

How to find the hard-iron effects are outlined in appendix A, according to the outline in [24].

Furthermore the magnetometer will be placed in an indoor envi-

ronment. Due to the amount of electronic equipment as well as steel material in the homes of today varying magnetic fields will be present throughout the rooms [25], [18]. Said variation in the fields can even be used for navigations by creating a map of the magnetic fields indoors [26].

These external fields will create soft-iron effects that will affect the measurement values. These can be modelled as a matrix, W^{-1} that is multiplied with the values and transforms them from the sphere of possible measurement values to an ellipsoid. The approach to estimate the soft-iron effects can be found in appendix A.

The corrected measurement values, B_c, supposing no misalignment, can then be obtained as:

$$B_c = W^{-1}(B_p - V) \tag{3.11}$$

with B_p being the uncorrected values and

$$B_c = \begin{pmatrix} B_{cx} \\ B_{cy} \\ B_{cz} \end{pmatrix}$$

The z-axis is by convention aligned with gravity, [8], [27], which means that the vertical component of the geomagnetic field vector will be measured by the z-axis. The horizontal component, then perpendicular to the z-axis, will be measured by the x- and y-axis, [24], as per figure 3.8.

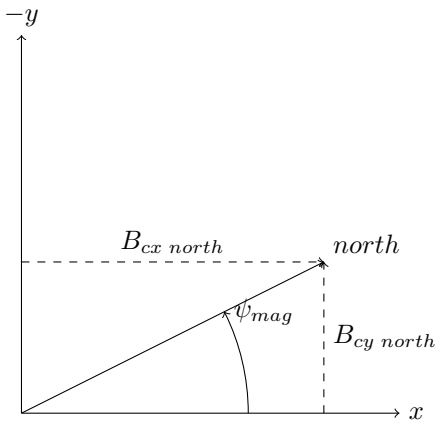

Figure 3.8: Magnetometer measurements of the plane perpendicular to gravity

The angle between the x-axis and magnetic north, ψ_{mag} can thus be calculated as

$$\psi_{mag} = tan^{-1}\left(\frac{-B_{cy}}{B_{cx}}\right) \tag{3.12}$$

What should be noted is that the angle ψ_{mag} differs from the angle ψ described in section 4 in that ψ is the deviation from when the door is closed while ψ_{mag} is the deviation from magnetic north. To find ψ from ψ_{mag} simply subtracting the initial angle of ψ_{mag} is sufficient, as can be seen in figure 3.9.

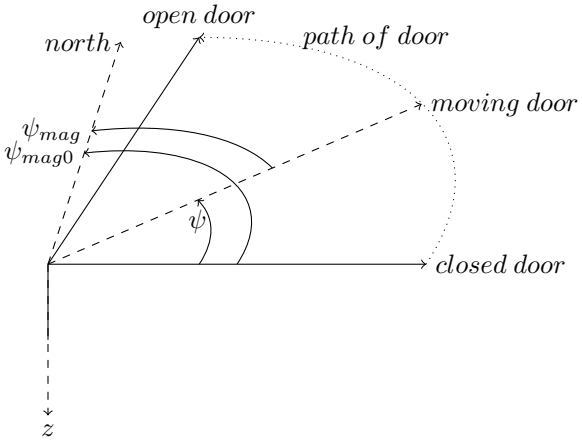

Figure 3.9: Difference between the angle actually measured by the magnetometer and the angle of opening of the door

The procedure outlined so far assumes perfect alignment of the device with gravity. This might not be the case, but can be compensated for. Including the derotation procedure of section 4.3 the complete correction of the magnetometer values are described by eq. (3.13).

$$B_c = R_y(\theta)R_x(\phi)W^{-1}(B_p - V) \tag{3.13}$$

B_c represents the corrected values, B_p the raw data, W^{-1} the soft-iron effects, V the hard-iron effects and $R_y(\theta)$ and $R_x(\phi)$ the roll rotation matrix and the pitch rotation matrix respectively [27],[24]. These last matrices representing the rotation of the device are more closely described in section 4.2.

3.3 Gyroscope

A gyroscope is basically a component that gives information of the angular displacement of an object. The operating principles behind these devices can vary, however the MEMS gyroscope, small enough to be interesting in many consumer applications, usually function using vibrations [28].

When small vibrating mechanical elements are rotated they experience so called Coriolis acceleration causing a transfer of energy between the vibrating modes. For instance so called tuning fork gyroscopes are based on a pair of masses that are oscillating with equal amplitude but in opposite directions. When subjected to the Coriolis force [1] due to rotation an orthogonal vibration appears, which can be sensed.

This might seem as the perfect device for the purpose of detecting the angle of the open door. However, due to the need for constantly vibrating components these devices are quite large power consumers. At normal operation the gyroscope consumes 6.1 mA [30], which can be compared with the consumption of the combination of the magnetometer and the accelerometer, being around 110 μA [6]. Comparing this to the magnet contact currently in use, with a consumption in the range of μA a consumption in the range of mA is clearly too large. Therefore the usage of the gyroscope is rejected.

[1] The Coriolis force is a force that affects objects on a rotating plane. As the outer parts of said plane will spin faster than the inner parts of the plane, movement in the plane will appear to be deflected for an observer in the plane. For an observer outside the rotating plane it will appear straight, as the deflection comes from the displacement at different speeds of the plane relative to the "straight" movement [29].

4. Frame of reference

4.1 Description

In the earlier description of the operation of the accelerometer it was assumed that it was correctly aligned with one axis in the direction of gravity, one completely perpendicular to the door and finally one perpendicular to the other two in the plane of the door. This might not necessarily be true. To be able to describe the rotation of the accelerometer three angles are usually defined [8],[27],[3],[31].

The angles, which correspond to the Euler XYZ-angles, are defined as

- **Roll,** ϕ, is referred to as the angle of rotation around the x-axis, according to figure 4.1.

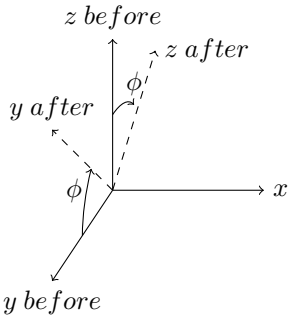

Figure 4.1: The roll angle

- **Pitch,** θ, is referred to as the angle of rotation around the y-axis, according to figure 4.2.

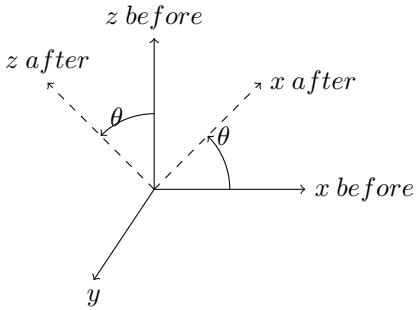

Figure 4.2: The pitch angle

- **Yaw,** ψ, is referred to as the angle of rotation around the z-axis, according to figure 4.3. Sometimes this angle is also referred to as the heading angle, for instance in aerospace technology [1].

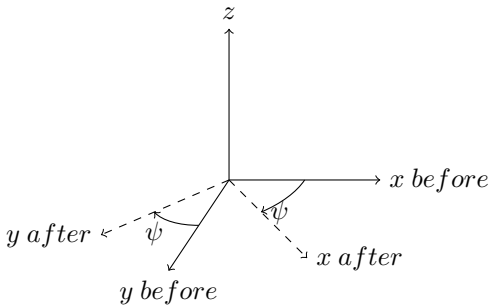

Figure 4.3: The yaw angle

The change in measurement values due to rotation of the device can be described by the following matrices [8],[27], [31] which differ in the definition of the directions of the θ and ψ angles in one of the sources.

$$R_x(\phi) = \begin{pmatrix} 1 & 0 & 0 \\ 0 & cos\phi & -sin\phi \\ 0 & sin\phi & cos\phi \end{pmatrix} \tag{4.1}$$

$$R_y(\theta) = \begin{pmatrix} cos\theta & 0 & sin\theta \\ 0 & 1 & 0 \\ -sin\theta & 0 & cos\theta \end{pmatrix} \tag{4.2}$$

$$R_z(\psi) = \begin{pmatrix} cos\psi & -sin\psi & 0 \\ sin\psi & cos\psi & 0 \\ 0 & 0 & 1 \end{pmatrix} \tag{4.3}$$

where $R_x(\phi)$ denotes the rotation around the x-axis, $R_y(\theta)$ the rotation around the y-axis and $R_z(\psi)$ the rotation around the z-axis.Together they form the complete matrix of rotation, R, giving full information on the rotation of the component relative to a known direction.

$$R = R_z(\psi)R_y(\theta)R_x(\phi) \tag{4.4}$$

This matrix is then multiplied with the measurement values to get the derotated values.

4.2 Finding the rotation

To be able to find the perfectly aligned measurement values of the magnetometer and the accelerometer it is important to derotate the component. Otherwise the measurement values for the acceleration of the door in the plane that is moving might have a component due to gravity which would result in too large values. Likewise the magnetometer can be affected.

For this purpose one must first find the current rotation of the coordinate system of the component in relation to gravity and magnetic north. Usually one assumes that the z-axis is aligned with gravity in the non-rotated coordinate system. This means that the gravity vector, G, in the derotated coordinate system can be described as [8],[27]

$$G = \begin{pmatrix} 0 \\ 0 \\ g \end{pmatrix} \tag{4.5}$$

where g denotes the gravity of the earth, which approximately corresponds to $9.82\frac{m}{s^2}$.

When the accelerometer is only affected by gravity, the effect of a certain rotation on the measurement values, G_r, can be described by eqs. (4.4) and (4.3), as per:

$$\begin{pmatrix} 0 \\ 0 \\ g \end{pmatrix} = RG_r = R_z(\psi)R_y(\theta)R_x(\phi) \begin{pmatrix} G_{rx} \\ G_{ry} \\ G_{rz} \end{pmatrix}$$

Since rotation along the yaw angle, ψ, will not affect the gravity measurements this rotational matrix can be removed from the equation.

$$R_z(\psi)^{-1} \begin{pmatrix} 0 \\ 0 \\ g \end{pmatrix} = R_z(\psi)^{-1}R_z(\psi)R_y(\theta)R_x(\phi) \begin{pmatrix} G_{rx} \\ G_{ry} \\ G_{rz} \end{pmatrix}$$

$$R_z(\psi)^{-1} \begin{pmatrix} 0 \\ 0 \\ g \end{pmatrix} = \begin{pmatrix} cos\psi & sin\psi & 0 \\ -sin\psi & cos\psi & 0 \\ 0 & 0 & 1 \end{pmatrix} \begin{pmatrix} 0 \\ 0 \\ g \end{pmatrix} = \begin{pmatrix} 0 \\ 0 \\ g \end{pmatrix}$$

$$\Rightarrow \begin{pmatrix} 0 \\ 0 \\ g \end{pmatrix} = R_y(\theta)R_x(\phi) \begin{pmatrix} G_{rx} \\ G_{ry} \\ G_{rz} \end{pmatrix} \quad (4.6)$$

Using eq. (4.1) and eq. (4.2) one can further relate the angles to the measurements.

$$R_y(\theta) * R_x(\phi) * \begin{pmatrix} G_{rx} \\ G_{ry} \\ G_{rz} \end{pmatrix} =$$

$$= \begin{pmatrix} cos\theta & 0 & sin\theta \\ 0 & 1 & 0 \\ -sin\theta & 0 & cos\theta \end{pmatrix} \begin{pmatrix} 1 & 0 & 0 \\ 0 & cos\phi & -sin\phi \\ 0 & sin\phi & cos\phi \end{pmatrix} \begin{pmatrix} G_{rx} \\ G_{ry} \\ G_{rz} \end{pmatrix}$$

$$\Rightarrow \begin{pmatrix} 0 \\ 0 \\ g \end{pmatrix} = \begin{pmatrix} cos\theta & sin\theta sin\phi & sin\theta cos\phi \\ 0 & cos\phi & -sin\phi \\ -sin\theta & cos\theta sin\phi & cos\theta cos\phi \end{pmatrix} \begin{pmatrix} G_{rx} \\ G_{ry} \\ G_{rz} \end{pmatrix}$$

From this one can see that the y-component of the real gravity vector is only affected by the roll angle, ϕ, enabling the determination of the roll angle.

$$G_{ry}cos\phi - G_{rz}sin\phi = 0$$

Resulting in the following expression for the roll angle:

$$\begin{aligned} \frac{sin\phi}{cos\phi} &= tan(\phi) = \frac{G_{ry}}{G_{rz}} \\ \phi &= tan^{-1}\left(\frac{G_{ry}}{G_{rz}}\right) \end{aligned} \tag{4.7}$$

Likewise the x-component of gravity gives the following equation

$$\begin{aligned} cos\theta G_{rx} + sin\theta sin\phi G_{ry} + sin\theta cos\phi G_{rz} &= 0 \\ \frac{sin\theta}{cos\theta} = tan\theta &= \frac{-G_{rx}}{sin\phi G_{ry} + cos\phi G_{rz}} \\ \theta &= tan^{-1}\left(\frac{-G_{rx}}{sin\phi G_{ry} + cos\phi G_{rz}}\right) \end{aligned} \tag{4.8}$$

which permits the calculation of the pitch angle, θ.

To finally determine the yaw angle the static accelerometer measurements can not be used, since they do not give any information about the rotation of the vectors perpendicular to gravity. To find this angle, which is the one of interest to this thesis, one instead needs to use the approach outlined in section 3.1.3 or 3.2.3.

4.3 Derotating the measurement values

Knowing the pitch and roll angles it is then possible to compensate for the misalignment between the measurement coordinate system and for instance gravity. Optimally one of the axes in said coordinate system should be aligned with gravity, in this case the pitch and roll angles would be 0.

However when this is not the case the knowledge of these angles can be used to transform the measurement values to their optimal equivalents. This is done by multiplying the sensor measurements by the rotation matrices, $R_x(\phi)$ and $R_y(\theta)$ from eq. (4.1) and (4.2). For instance the accelerometer measurements, a are thus derotated, giving the corrected values of a_c as shown in eq. (4.9).

$$a_c = R_y(\theta)R_x(\phi)a \tag{4.9}$$

Note that this differs from eq. (4.4) in that the matrix $R_z(\psi)$ is not included. This is because the misalignment of the yaw angle, which would correspond to the coordinate system not being aligned to a certain heading angle will not affect the static accelerometer measurement values. This is shown in eq. (4.6).

Therefore the derotation is only performed in relation to gravity and not in relation to north. This is because the yaw angle, ψ, is unknown and is what this thesis hopes to determine.

One could assume that a slight misalignment with the plane of the door would affect the measured accelerations due to movement, but since said acceleration is already small in comparison to gravity these effects are considered to be very small and are therefore neglected.

4.3.1 Derotating to find the magnetometer angle

In the case that one measures the magnetic fields and not the acceleration the horizontal axes cannot be considered to be 0, as in eq. (4.6) for acceleration. The magnetic values corrected for pitch and roll rotation, B_c can then be expressed as in eq. (4.10)

$$B_c = R_z(-\psi)B = \begin{pmatrix} cos\psi & sin\psi & 0 \\ -sin\psi & cos\psi & 0 \\ 0 & 0 & 1 \end{pmatrix} \begin{pmatrix} B_x \\ B_y \\ B_z \end{pmatrix} \tag{4.10}$$

where B corresponds to the measurements aligned with north. Knowing that the geomagnetic field has an angle of inclination, δ, being the difference between the geomagnetic field vector and the horizontal plane, B can be described by eq. (4.11), [27].

$$B = \begin{pmatrix} B_0 cos\delta \\ 0 \\ B_0 sin\delta \end{pmatrix} \tag{4.11}$$

B_0 represents the size of the geomagnetic field. The values are here considered to be derotated when B_x is aligned with north. Combining eq. (4.10) and eq. (4.11) gives eq. (4.12).

$$B_c = \begin{pmatrix} cos\psi & sin\psi & 0 \\ -sin\psi & cos\psi & 0 \\ 0 & 0 & 1 \end{pmatrix} \begin{pmatrix} B_0 cos\delta \\ 0 \\ B_0 sin\delta \end{pmatrix} \tag{4.12}$$

which gives

$$\begin{pmatrix} B_{cx} \\ B_{cy} \\ B_{cz} \end{pmatrix} = \begin{pmatrix} B_0 cos\delta cos\psi \\ -B_0 cos\delta sin\psi \\ B_0 sin\delta \end{pmatrix} \tag{4.13}$$

which firstly shows, as expected, that the axis parallel to gravity, z, corresponds to the vertical component of the geomagnetic field. Secondly it shows that the yaw angle can be calculated as eq. (4.14).

$$\begin{aligned} B_{cx} &= B_0 cos\delta cos\psi \\ B_{cy} &= -B_0 cos\delta sin\psi \\ \Rightarrow \frac{-B_{cy}}{B_{cx}} &= \frac{-(-B_0 cos\delta sin\psi)}{B_0 cos\delta cos\psi} = \frac{sin\psi}{cos\psi} = tan\psi \end{aligned}$$

thus

$$\psi = tan^{-1}(\frac{-B_{cy}}{B_{cx}}) \tag{4.14}$$

which corresponds to the previously found expression for the magnetic yaw angle, as per eq. (3.12).

5. Algorithm

To learn how much the door is open, including whether it is open at all, an algorithm is implemented based on the theory of previous sections. Since the accelerometer is very susceptible to noise, some kind of filtering is also needed to obtain reliable results. As the accelerations measured tend to be quite small, around 5% of gravity, a correct implementation of said filtering is of utmost importance. An overview of the algorithm is described in the flowchart of figure 5.1 below. Note that the green rectangle represent the calibration, while the blue blocks represent the continuous calculations during operation in field. The rhombic shapes represent decisions, meaning the control of certain conditions to execute parts of the code.

For the stationary parts of the algorithm, defined by the standard deviation being below the threshold, the angle is determined by the magnetometer measurements. However, as the magnetometer is sampled at a much lower rate than the accelerometer, to save power, it will not detect the fast opening of a door until the next measurement event. Therefore the accelerometer is considered to be able to faster detect that the door is being opened, if movement is detected. This is the reason for the accelerometer angle to only be corrected using the magnetometer when stationary.

As can be noted below the door is considered to be open if the angle of the door is larger than 2 degrees. The reason for this value (as opposed to 0 degrees) is that there is some inaccuracy in the values and a slight range is needed to prevent false positives, that is false conclusions that the door would be open.

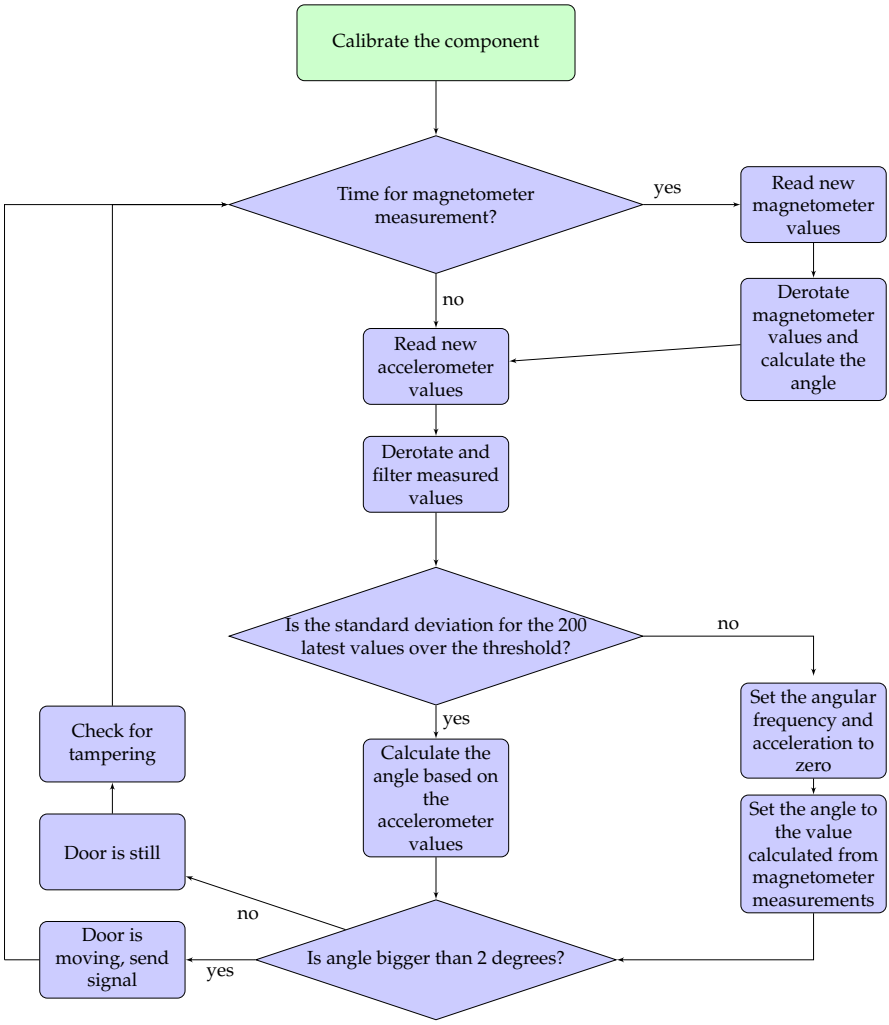

Figure 5.1: A flowchart of the implemented algorithm

Further explanation of the included steps can be found in the following sections.

5.1 Calibration

The first step of the algorithm includes the calibration of the components. The hard-iron effects can be calculated at the circuit board assembly, since they are unaffected by surrounding magnets. However, soft-iron effects can not be compensated at the factory, since they are dependent on the environment the circuit board is placed in, as described in section 3.2.2. Neither can the determination of the rotation of the device. Likewise the standard deviation for the threshold to be used later in the algorithm is calculated when the component is mounted on its final place.

Although the device is factory calibrated to show the correct accelerometer and magnetometer output, the mounting procedure of the device might affect these values slightly, as mentioned in section 3.1.2. For maximal precision further calibration is required. During this procedure the scale-factors, being a constant multiplicative error factor, and the offset, being the difference between output value and 0 when the input is 0, are recalculated. These can be calculated at the place of mounting the components on the circuit board.

Furthermore some additional magnetic fields might exist in the surroundings of the door. These can vary over the distance of the open door, causing the magnitude of the calculated angle to be slightly off. Therefore a scale factor for the magnetometer angle, yaw, is also calculated. To be able to detect possible tampering the maximum and the minimum of the measured magnetic field is also noted. During the entire calibration so far the magnetometer is sampled with quite a high sampling frequency to avoid missing any extreme values. For the rest of the algorithm this is not necessary and the sampling frequency and output data rate (ODR) is lowered.

When all this is done the initial value of the magnetometer angle for the closed door relative to north is calculated, which is used to express the following angles as relative to the closed door.

The entire process is shown in the flowchart of figure 5.2 below. Note that the round bubbles represent steps possible to do at the factory producing the circuit board and the rectangles represent actions to be performed at the installation spot of the device.

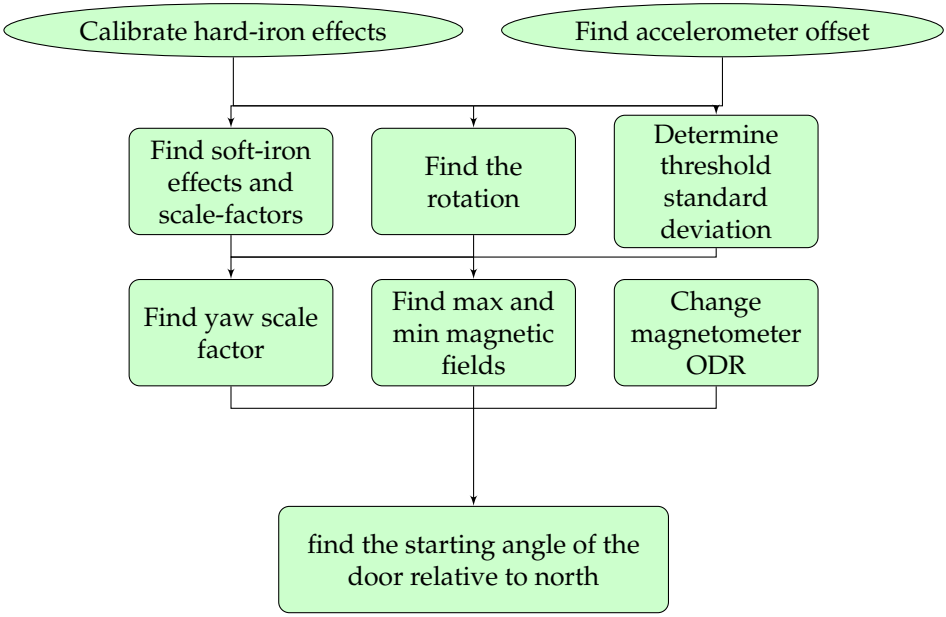

Figure 5.2: A flowchart of the calibration of the device

The procedure for these different calibrations are further described in the following sections.

5.1.1 Finding hard-iron offsets

The mathematics for finding the hard-iron effects can be viewed in appendix A. There it is shown that a vector of several magnetometer values are required to be able to perform least squares optimisation and find the hard-iron effects. For optimal results the examples should be as varying as possible [24], [18].

Therefore the device is rotated in all possible directions, especially around the different axes of the magnetometer coordinate system. During this rotation procedure data is collected to map as large a part of the sphere of possible measurement values as possible. This requires a sufficient sampling rate as not to miss too many directions.

Using the measured values, the hard-iron effects can thus be calculated as per appendix A.

This method however requires performing the inverse matrix operation, which is a relatively complex function. For certain applications this might be too power consuming, even though it is only performed during installation. One could therefore utilize a less power consuming approach, based on viewing the hard-iron effects as the geometrical displacement of the centre of a sphere. By rotating the device and noting the extreme values in each direction one can thus calculate the centre of said sphere, a illustrated in eq. (5.1) for the x-direction, [18].

$$V_x = \frac{max_x + min_x}{2} \tag{5.1}$$

Here V_x represents the centre in x-direction, corresponding to the hard-iron effects and max_x and min_x represents the maximum and minimum values respectively of the magnetic field in x-direction. Here one only needs to store the current maximum and minimum of each axis, which means that considerably less memory is needed than for the more complex function.

What should be noted is that these biases might be around the size of the geomagnetic field. Even though they can be removed by the software the actual sensor will still measure them. This means that the range of the sensor must include the geomagnetic field in combination with the hard-iron effects. However increasing the range of the sensor naturally decreases the sensitivity, as the same amount of bits in the processor memory now represents a larger range. It is therefore desirable to decrease the hard-iron effects as much as possible even though they can be filtered by the software.

5.1.2 Finding soft-iron effects and scale-factors

As for the soft-iron effects they can be compensated for according to the mathematical outline of appendix A. What is needed for this method is firstly correctly calculated hard-iron effects and secondly a set of tri-axial measurement values. When this is obtained the soft-iron effects can be calculated with the help of inverse matrix operations and the usage of eigenvectors. Since the effects of incorrect scale factors will be indistinguishable from the soft-iron effects these will also be compensated for by this approach.

However, the usage of said matrix operations is relatively complex and alternative ways of finding these effects might be required

in certain applications. One way of achieving this is by using a more geometrical approach. Knowing that the soft-iron effects will turn the sphere of measurement values into an ellipsoid, one can try to map said ellipsoid by rotating the component and noting the magnetic field in all directions. By assuming that the ellipsoid is more or less aligned with the coordinate system, and that the real size of the sphere is consistent with the geomagnetic field, the scaling factors of each axis can be calculated. This is simply done by dividing the true radius (the geomagnetic field), with the semi-axes of the ellipsoid, as per eq. (5.2). The semi-axes of the aligned ellipsoid is found by taking the distance between the extremes of every semi-axis and dividing by 2 [32].

$$W_x = \frac{B_0}{\frac{max_x - min_x}{2}} \tag{5.2}$$

Here W_x represents the scaling factors in the x-direction and max_x and min_x represents the maximum and minimum values of the magnetic field in x-direction respectively.

The downside of this method however is that it is dependant on the magnetic field remaining fairly constant over time. For the application described herein the component will be placed in an indoor environment. Normally there are several electric components in residences that can cause additional magnetic fields. This means that the measured magnetic field of the component will vary. As several measurement points in multiple directions are required to ensure that the maximum and the minimum are found, this will only be correct for the initial magnetic field where the calibration took place. For the other magnetic fields along the path of the door only one set of measurements are taken, thus rendering it impossible to counter the variations in the magnetic fields.

As for the more complex ways of calculating the soft iron effects they also compensate for the scale factors arising from the mounting of the device.

5.1.3 Finding accelerometer scale-factors and offsets

For maximum accuracy of the measurements the accelerometer scale factors are also calibrated. One way of achieving this is to rotate the device and take accelerometer measurement values at different directions. The absolute value of each set of measurement values should

always correspond to gravity, supposing the device is not rotated too quickly. Should the scale factors be incorrect the gravity sphere might be transformed into an ellipsoid, similar to the soft-iron effects. This can be countered by using the normal equation for least squares optimisation as in eq. (A.8).

Another way to find the scale factors is to place the accelerometer on a flat surface and measure the gravity, which should correspond to 1 g in one axis and 0 g in the others. The device is thereafter rotated 180 degrees, so that the axis sensing gravity is turned upside down. Said axis should now measure -1g. The scale factor, sometimes referred to as gain [33], of this axis can now be calculated the same way as for the magnetometer scale factors [11].

$$scale\ factor_x = \frac{max_x - min_x}{2} \tag{5.3}$$

The same procedure is then repeated for the other axes.

To find the accelerometer offsets the device is mounted on the door and derotation and scaling is performed. The resulting accelerometer values are then considered to be the offsets. This does mean that the gravitation is considered to be an offset, but since it is constant while the component is attached to the door it should not change anything.

Usually accelerometer offsets are calibrated the same way as for the magnetometer, according to eq. (5.4) [33].

$$offset = \frac{max_x + min_x}{2} \tag{5.4}$$

However, as the accelerometer is mounted on a door and will hopefully not move from there this has not been deemed necessary, as only the offset for the current mounting is relevant.

5.1.4 Finding yaw-scaling

As the soft-iron effects might not be completely successfully filtered, neither by the more complex function or the simplified version, the resulting yaw angle might be incorrectly estimated. In assuming a stationary field at every point of the path of the door the estimated effects of this field on the measurements at a certain point will remain the same independently of the time. Supposing that the effect on the

calculated yaw angle is more or less linear, one could envision the error at any given point to simply be a multiplicative factor.

To find this factor the starting angle, ψ_0 is first determined. This is simply the angle relative to north of the closed door. Thereafter the door is opened $90°$, at an angle ψ_{90}. Knowing that this distance should correspond to a quarter of a circle the difference between these two angles is then used to calculate the yaw scaling according to eq. (5.5).

$$(\psi_{90} - \psi_0) yaw\ scaling = 90° \tag{5.5}$$

$$yaw\ scaling = \frac{90°}{\psi_{90} - \psi_0} \tag{5.6}$$

5.2 Filtering

As the accelerometer values are integrated at least one time the errors in the initial acceleration values will propagate to the angle determination. A good filtering algorithm is therefore required.

Since the signal level of the accelerometer is quite low in relation to the noise the performance of the accelerometer algorithm is heavily influenced by the choice and implementation of a filtering algorithm. However, said algorithm will be implemented on a small processor on a device powered by a battery, which means that the power consumption of the processor running the algorithm also plays a part. Therefore there will be a trade-off between finding as good a filtering algorithm as possible and minimising the power consumption.

No white-noise filtering is used for the magnetometer measurements, due firstly to the fact that measurements show that the white noise levels are quite low in relation to the signal and secondly to the fact that the sensor values are not integrated, so the errors do not propagate.

5.2.1 Moving average filtering

One of the simplest algorithms consists of using a simple moving average filter. In this case the value at each place in the measurement series is replaced by the average of a certain number of values surrounding said value. With a number, n, of measurement values, $x_1 ... x_n$ from a certain measurement series, the resulting filtered value, y, would be

$$y = \frac{1}{m}x_1 + \frac{1}{m}x_2 + ... + \frac{1}{m}x_n \tag{5.7}$$

where m is a number specified by the implementer and should be equal to n for the algorithm to return the correct magnitude of the filtered value. This algorithm can also be more compactly described as [34]

$$y = \frac{1}{m}\sum_{k=1}^{n} x(k) \tag{5.8}$$

The number of samples chosen, n, often called the window size, will here have a big importance on the resolution of the filtered measurement values.

The simplicity of this algorithm, only requiring n additions and 1 division per sample makes it an attractive algorithm due to the low power requirements. Since the noise, as noted earlier, is mainly distributed as white noise average filtering generally gives a good view of the assumed original signal.

This is the filtering used in the final version of the algorithm due to its simplicity.

5.2.2 Frequency filtering

Another way of removing the noise from the signal is to apply a filter in the frequency domain. Since the random white noise is distributed all over the frequency spectra, but the signal sampled at a moderately high sampling rate does not have any sharp peaks, a low-pass filter seams ideal to remove the noise. One could also envision trying to find recurring frequency components of the signals, especially after viewing the spectrograms of the signal, see figure 6.7. However these slightly more intensive frequencies seem to differ from door to door and be more related to vibrations when closing the door than to the accelerations of the movement. If one could find said frequency ranges it would be possible to implement a band-pass filter. However that would require knowledge of the certain frequency for the vibration when closing a particular door. This has not been found at the moment.

Therefore it appears that the best option is to use a low-pass filter. For the purpose of simplicity the current implementation, as a proof of concept, uses a very simple algorithm where a vector of ones and zeros is multiplied with the measurement vector in the frequency domain. All but the lowest frequencies of the signal are thus set to zero. When the resulting vector is then returned to the time domain using an inverse Fourier transformation the spikes and the high frequency noise is thus removed.

The beauty of using low-pass filtering is that it is easily implemented and does not take a lot of processor power, while giving sufficient results. In a real hardware application this kind of filtering might not be implementable, but as a proof of concept only implemented with software it works quite well.

5.2.3 Wavelet filtering

Another way of utilising the fact that the noise can be found all over the frequency is the use so called wavelet filtering. Here the signal is decomposed in the frequency domain into a high-frequency part, that contains the detailed parts of the signal, and a low-frequency part, containing the approximation coefficients. Each part can then be further decomposed into a low frequency and a high-frequency part, which in turn can be decomposed [35]. To obtain information about both the time and frequency different sized windows (amount of samples filtered at the same time) are used in the time domain. For the high frequency part a smaller window is used to obtain good time resolution and for the low frequency part a larger window is used to obtain reliable information about the frequency.

The discrete wavelet transform (DWT) can thus localize a signal in time and scale, unlike the discrete Fourier transform which localizes signals in the frequency domain. The DWT is obtained by filtering using a series of filters with different scaling functions, where the scales are simply different lengths of the filters, obtained by sampling [35]. This means that information can be lost due to sampling at a lower rate.

The filter depends on the wavelet, sometimes referred to as the mother wavelet [36]. This wavelet is then used to build up the different components of the decomposed signal to give the filter coefficients. The scale function and the wavelet of the Haar wavelet system are shown in figure 5.3. This can be considered the easiest mother

wavelet to use since it consists of a simple step-function.

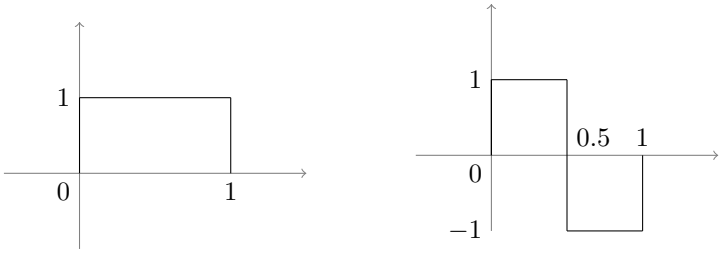

(a) Scaling function (b) Wavelet

Figure 5.3: Haar wavelet system, showing the scaling function and mother wavelet.

The signal can then be reconstructed after decomposition. However, to smooth or filter signals one can choose not to include the highest frequency components or components with too low a contribution.

5.3 Zero Velocity Compensation

Even with a good filtering algorithm certain (hopefully small) deviations from the real signal will exist. During integration from angular frequency to angle, as per eq. (3.9), these deviations will be magnified. In the case of the tangential version an integration from angular acceleration to angular frequency is also required. This double integration greatly increases the error. Since the direction of the radial angular frequency is determined by the direction of the tangential equivalent, any error in sign of the tangential angular frequency is transferred to the radial version

Furthermore varying offsets of the accelerometer might arise if the accelerometer happen to be changing tilt ever so slightly. Likewise if the noise is not uniformly distributed across the signal, this will appear as a bias. None of these errors will be removed by using a filtering algorithm based on removing white noise. Therefore an algorithm with some form of verification of the values and some kind of compensation for the errors arising is required.

When the velocity has been corrected the angle can be recalculated using the modified velocity values, improving the accuracy of the angle determination.

5.3.1 Description

The problem of integrating errors exists for different implementations of accelerometers. For a pen with tilt sensing in an IMU, writing digitally without ink, Samsung has developed an algorithm, [31], [8], referred to as zero velocity compensation, ZVC, to determine when it is still and when it is moving. In this algorithm it is assumed that when writing it is impossible to have a constant velocity of the pen. Thus when the acceleration is zero the pen is still between the strokes of writing a letter[15]. It is here assumed that there is a small pause when the pen is motionless between strokes.

When the acceleration is zero the velocity should therefore be zero. The deviation from zero of the velocity at this point is therefore considered to be erroneous. By modelling the error, e, as linear it is possible to correct for an offset in the acceleration, a, causing the velocity, v, to grow over time[15]. The error, corresponding to the slope of the linear erroneous curve, is found by dividing the velocity at stand-still with the number of samples during the movement period. During the moving period the velocity is then corrected by subtracting the error multiplied with the number of samples since the last stand-still. This is described by eq. (5.9). For sample number k, in the moving region, where the movement stops at sample k_2 and starts at sample k_1:

$$e = \frac{v(k_2)}{k_2 - k_1} \tag{5.9}$$

$$v(k) = v_0(k) - e * (k - k_1) \tag{5.10}$$

$$a(k) = a_0(k) - \frac{e}{\Delta t} \tag{5.11}$$

where Δt is the sampling time, $a(k)$ and $v(k)$ the corrected acceleration and velocity value respectively at time k and $a_0(k)$ and $v_0(k)$ the uncorrected acceleration and velocity value respectively. The reason for the division with Δt for the acceleration error is due to the error being linear in velocity. The slope of this error with respect to time would then correspond to the bias in acceleration. However since the error, e, is only the slope relative to the number of samples, the division by t is needed to relate the slope to time.

5.3.2 Implementation for the movement of a door

ZVC can also be used for the purpose of detecting the movement of the door. Under the assumption that one does not open a door with constant velocity (which is reasonable if one does not sneak the door up entirely, in which case the acceleration would still be too small for the accelerometer to notice) all cases of zero acceleration correspond to the door being still.

For the door the ZVC will work according to eq. (5.9)-(5.11) for the tangential component of the centripetal acceleration. The acceleration, a, described by eq. (5.11) will here correspond to measured tangential acceleration divided by the radius and the velocity will represent the angular frequency, ω.

For the radial component the relation between the angular frequency and the acceleration is not a simple integration, instead, as represented by eq. (3.5), the acceleration is the squared angular frequency times a factor. This means that an error, a_{err} in the acceleration at time k would propagate to the angular frequency, ω_{err}, according to

$$(a(k) + a_{err}(k)) = -(\omega(k) + \omega_{err}(k))^2 R \tag{5.12}$$

$$|\omega(k) + \omega_{err}(k)| = \sqrt{(\frac{a(k) + a_{err}(k)}{R})} \tag{5.13}$$

where a represents the correct acceleration, ω the correct angular frequency and R the radius of the angular movement.

When the angular frequency should be 0, in a stationary position at time k_2, the error, e, is simply

$$e = \omega(k_2) + \omega_{err}(k_2) = \omega_{err}(k_2) \tag{5.14}$$

The reason for this error to not be divided by the length of movement, as eq. (5.9), is that it is not cumulative. This is because the angular frequency, according to eq. (3.7) does not depend on earlier values of said frequency. The correction terms at time k for the sequence of movement is thus described by eq. (5.15), using eq. (5.12).

$$\begin{aligned} \omega(k) &= \omega_0(k) - e \\ a(k) &= a_0(k) + e^2 R \end{aligned} \tag{5.15}$$

where ω_0 and a_0 are simply the uncorrected values.

What is worth noting is that the error is here assumed to be a constant bias for the acceleration, which might not necessarily be true. For the radial angular frequency the error then becomes a constant bias as well, while it becomes a linear multiplicative factor for the tangential angular frequency due to the integration.

5.3.3 Detecting movement

In this zero velocity compensation algorithm it is vital to detect when the acceleration is zero, as this is the basis for the compensation. To do this different approaches can be tried. In [31] and [8] the standard deviation of the measurement is used as a verification measurement. If the standard deviation of a window of S samples at time k is higher than a predefined threshold the accelerometer is considered to be moving. Likewise when the standard deviation is below this threshold the accelerometer is considered to be still. Standard deviation, σ, for a vector, X, being defined as [37]

$$\sigma = \sqrt{E(X^2) - E(X)^2} \tag{5.16}$$

where E(X) is the expected value of X.

This approach can also be applied to a door. However, at times the vibrations of the door, arising from friction against the door frame among other things, will cause the standard deviation to be very high even though the absolute value of the acceleration from movement is very low. If the movement of the door is just starting or stopping this is not really a problem as there will only be incorrectly detected movement for the duration of the biggest vibrations, which tend to last some second. As the door is typically moving around 5 s an extra second will not make much of a difference.

However if some kind of trigger is supposed to be sent when movement is detected this might be problematic as this would cause false triggers to be sent when someone is, for instance, hammering. To counter act this the absolute value of the filtered acceleration could be used as well to determine whether the door is actually moving or not.

Since the peaks of vibration when closing the door are so much higher than those arising from simple acceleration of the door one can use the standard deviation to find where to apply a more brutal filter.

The need for a varying strength of the filter comes from the fact that the magnitude of said peaks cause them to not be properly dampened by the filtering algorithm used for the rest of the signal.

Another way of detecting movement is to look at the absolute value of the filtered accelerometer measurements. However since the errors include an offset of the accelerometer measurements they do not necessarily have an average value of zero. This could also cause false triggers of movement for an unmoving door. Furthermore real movement might be incorrectly classified as static since the entire curve could be displaced.

5.4 Connecting the component measurements

Originally the plan of this thesis was to only use an accelerometer, as described in section 5.4.1, however due to the possible drift, uncertainties of the position and difficulties in detecting small accelerations another component has been included for verifications (also tried in literature [25]), namely the magnetometer.

5.4.1 Accelerometer alone

To be able to find good curves for the angle calculated using the accelerometer measurements, certain assumptions need to be made to perform the corrections. Firstly it is assumed, as described in section 5.3, that the velocity is zero when no movement is detected. Secondly it is assumed that the local minima of the curve of the angle correspond to the door being closed. In the same way that error correction is performed, as described in eq. (5.9) - (5.11), correction for the erroneous angle is here performed for the samples between the local minima.

With this method it has been shown (see section 6.3.1) that it is not possible to surely ascertain whether the assumed closed position, arising from when the door is still, actually corresponds to a closed door instead of a door left slightly ajar.

5.4.2 Correction using the magnet contact

The uncertainties of the positions mentioned above necessitates some form of additional verification of the angle. One way of verifying if

the door is actually closed is to use an existing magnet contact as verification.

When the device is still and the magnet contact has confirmed that the door is closed two things happen. Firstly, zero velocity compensation is used to compensate for the drift in velocity. Secondly a kind of position correction is performed. This version of verification can ascertain whether the unmoving door is actually in a closed position or simply left ajar, enabling the correction of the angle for only the closed doors.

5.4.3 Correction using the magnetometer

Since the entire point of using an accelerometer is to replace the magnet contact another form of verification is needed. For this a magnetometer is chosen. Unlike the magnet contact it can provide information on the angle of the door at all positions.

Here the ZVC compensation is firstly performed, as usual, thereafter the angle is recalculated. As soon as the door is found to be still the angle of the accelerometer measurements is compared to the angle from the magnetometer. The magnetometer angle is always considered to be correct and the deviation of the accelerometer measurements angle is considered to be erroneous. This error, e, is then compensated over the entire movement sequence of the door, from k_1 to k_2 as per eq. (5.17).

$$e = \frac{pos(k_2)}{k_2 - k_1} \tag{5.17}$$

$$pos(k) = pos_0(k) - e * (k - k_1) \tag{5.18}$$

where k is the current time, pos is the angular position after correction and pos_0 the initial angular position. Notice the similarities to the ZVC.

Implementing this on a processor without access to memory containing the sequence of movement the accelerometer angle is simply set to the magnetometer value.

5.5 Adaptation to implementation on a processor with limited memory

The algorithm described above has been developed using a computer, however the provided circuit board with the accelerometer and magnetometer only include a cortex-M4 core processor, with considerably less computer power. Therefore some adaptations are required. Basically all of these modifications come down to power savings.

5.5.1 Compensating the ZVC

Firstly the ZVC will not be performable. This is due to the fact that the ZVC requires storage of all values during the time that the door is moving. Usually this corresponds to some second, but it might be moving quite a while longer. As the exact time needed to store a full sequence of movement is unknown it is not possible to create a structure in the processors memory to store all these values. One option could be to create an overly sized array to ensure that all the values would fit, however the usage of those amounts of memory space consumes a lot of power. This makes it too inefficient to use the ZVC in the form described in section 5.3.

Instead some form of adaptation without memory storage is required. This has been implemented by not performing the velocity compensation. The check for movement is still performed, but no correction is done for past values. Instead the angular frequency and acceleration is set to 0 and the angle is calculated based on these values of the angular frequency. Thus the value of the angle remains constant when no movement is detected. The difference being that no compensation is done in retrospect. With these modifications the algorithm is transformed into eq. (5.19).

$$\begin{aligned} &while\ stationary \\ &a(k) = 0 \\ &v(k) = 0 \\ &pos(k) = pos(k-1) \end{aligned} \tag{5.19}$$

This will lead to a risk of the angular frequency being erroneous during the entire movement sequence, especially if it does not go to 0

when the movement ceases. This will in turn cause the angular position to be incorrect. Therefore an additional verification is needed of the angular position, preferably during stationary periods, since the door, when closed, should be stationary. This is done by simply setting the angle to the magnetometer angle value.

5.5.2 Avoidance of memory storage

Except the memory required for the ZVC there are also other arrays that would preferable be saved when the amount of computer power of a PC is available. For instance to determine the standard deviation threshold the sums are directly used, as outlined in appendix B. Should a PC be available one could store the acceleration values in a vector and calculate the standard deviation of the vector.

For the moving average filtering only 1.3 seconds worth of samples are stored, corresponding to approximately 3.2 kB of data if the values are saved in the double format. This can be decreased to even further save memory, by limiting the samples saved or saving them in a shorter format. However, the reduction of samples stored decreases the efficiency of the filtering algorithm and using smaller formats can limit the accuracy.

5.5.3 Finding hard and soft-iron effects

The complex version of finding the soft and hard-iron effects requires the usage of inverse matrix functions, as well as finding the eigenvalues and eigenvectors of a matrix. For the soft-iron effects these are calculations that are repeated for every measurement point. This kind of complex calculations require some computer power.

As described in section 5.1.1 and 5.1.2 there are simpler and less exact ways of compensating these effects. For the kind of processor used in this work the more low power calculations of the simplified calibration method is thus used.

5.5.4 Sampling rates

One big source of power consumption is the sampling. By decreasing the sampling rate one can effectively decrease the power consumption. This has its disadvantages though, as the acceleration when opening the door can have a very short duration, where the time to reach maximum acceleration can be in the range of 0.2 seconds. With too low a

sampling frequency it is possible to miss this event. As the accelerometer is very good at conserving power a slightly higher sampling rate might be acceptable.

The magnetometer on the other hand is mostly used for verification of the angle in stationary positions and can therefore be sampled at a relatively low rate. In this thesis a sampling rate of 0.75 Hz has been used, but an even lower rate would be possible.

Simplifying the algorithm even further would also lower the current consumption.

5.6 Detection of tampering

Since the magnetometer measures the magnetic field one could envision an attempt to fool the algorithm by the usage of a strong external magnet. The benefit of this would then theoretically be that you could open the door while keeping the measured angle relative to north the same. To achieve this one would need to either add an additive magnetic field in one direction or add a negative field in the other direction, as can be seen in figure 5.4.

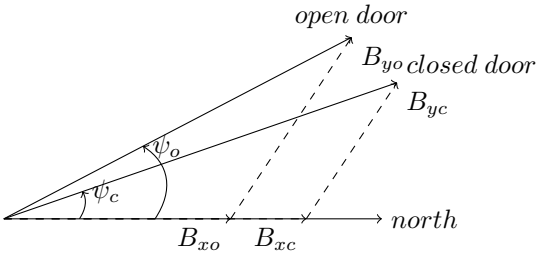

Figure 5.4: Opening of a door with no tampering attempt, that is no added field. Here o and c represents open and closed respectively.

Note that the resulting angle of the opening of the door is calculated as the difference between the current angle of the door and the original angle of the door. Thus with added additive magnetic field the situation would look as depicted in figure 5.5.

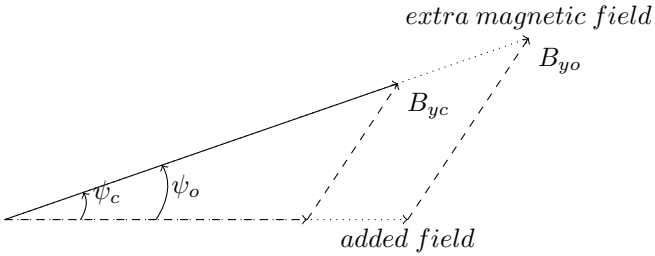

Figure 5.5: Opening the door during a tampering attempt, with an added magnetic field.

As can be seen the angle of the door would then appear to be the same for the open and closed door. Here a field has been added in x-direction, but one could also keep the angle of the door the same by adding a negative field in y-direction to decrease the size of this component. In both of these cases the size, or absolute value, of the magnetic field would change, depicted as the hypotenuse in figure 5.5. By simply controlling the absolute value of the magnetometer measurements tampering can thus be detected.

5.7 Window opening in the plane of gravity

The description up till now has been valid for a door or a window that is moving in the plane perpendicular to gravity. Some windows however are opened by rotating around an axis perpendicular to gravity. Since the accelerometer is especially sensitive to changes in gravity this can be calculated. By setting the angle of opening to be noted as θ, the different states can be described as in figure 5.6.

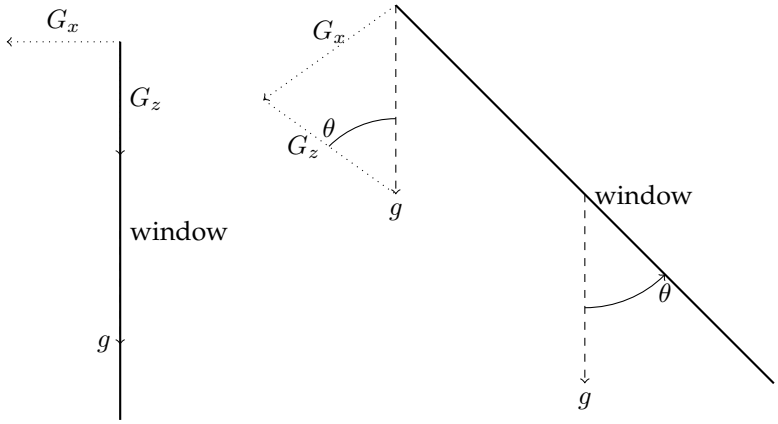

(a) Closed window (b) Open window

Figure 5.6: Open and closed state of a window that opens by rotating in the horizontal plane.

Here g represents gravity, and G_x and G_z the x- and z-axis measurement respectively. Using the same approach as in section 3.2.3, since only the component of the measurement parallel with gravity will be measured, an expression for the angle can be determined. This is shown in eq. (5.20).

$$\psi = tan^{-1}(\frac{G_x}{G_z}) \tag{5.20}$$

For increased accuracy the derotation procedure of section 4.3 can be applied.

One could also filter these values, however since no integration step is required and they do not depend on earlier measurements, they

will be much less susceptible to noise and this might be superfluous.

As the algorithm otherwise is developed for a door that is opened perpendicular to gravity, this is not included in the current algorithm, to save code as well.

6. Results

6.1 Accelerometer

6.1.1 Raw data

For the measurement series of this section the door was opened approximately $90°$ and thereafter closed. A process which was repeated number of times. Also angles different than $90°$ were tried. An example of the raw data for the accelerometer measurements can be viewed in figure 6.1.

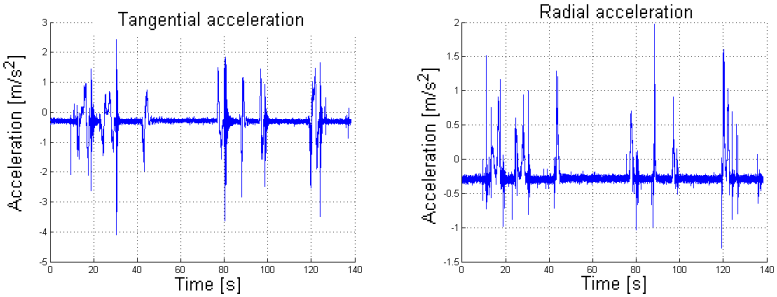

(a) Tangential acceleration

(b) Radial acceleration

Figure 6.1: Acceleration when opening and closing a door several times without any filtering.

Here the door was opened and closed at approximately 17s, 25s and 122s. At around 42s the door was also opened and not closed until 76s. Likewise a longer period of opening took place between approximately 88s-98s. As can be seen both these series of measurement values are subjected to a slight offset since they are not centred around the zero level. In addition the BNEA, white noise, is visible as the variations in the value between the clear peaks. Some of the peaks, such as the largest, can be seen to be very sharp without any change in the average value of the acceleration. These peaks are likely due

to the vibrations from friction with the door frame when opening or closing the door. This can also be viewed in the vertical acceleration measurements, as shown in figure 6.2.

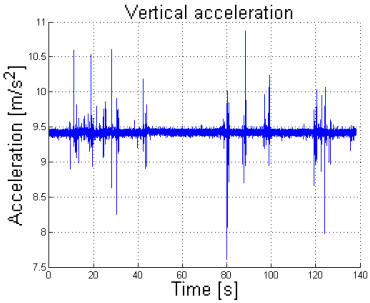

Figure 6.2: Vertical acceleration when opening and closing a door several times without any filtering.

As can be seen here only the white noise and the peaks due to friction are visible.

When calculating the angular frequency from the radial acceleration, using eq. (3.7), it looks approximately the same as the acceleration curves. However when calculating the angular frequency using the tangential acceleration and eq. (3.8), some white noise is filtered due to the integration step, but the curves quickly drift away due to the offset when integrating. This is shown in figure 6.3.

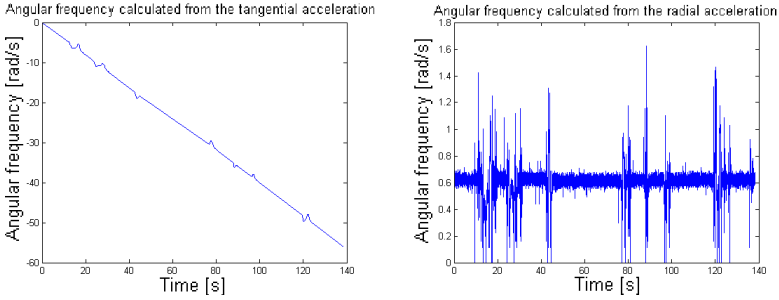

(a) Tangential version

(b) Radial version

Figure 6.3: Angular frequency when opening and closing a door several times without any filtering.

As can also be seen the sign of the angular frequency can not be derived solely from the radial acceleration. What is shown in these curves is the absolute value of the angular frequency. In the algorithm this is compensated for before calculating the value.

6.1.2 Filtering

To get a clearer image of the actual signal by removing the white noise it is necessary to perform some kind of filtering.

6.1.2.1 Moving average filtering

The easiest way of doing this is to perform moving average filtering. The result for averaging over 1 second with a sampling rate of 200 Hz is shown in figure 6.4.

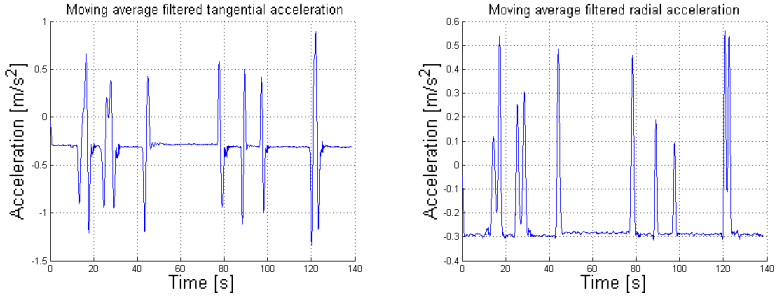

(a) Tangential acceleration

(b) Radial acceleration

Figure 6.4: Moving average filtered acceleration when opening and closing a door several times.

As can be seen the big friction peaks are now gone, as is the most of the white noise. However the offsets are still there. Performing the same filtering on the vertical signal keeps it fairly constant, as shown in figure 6.5.

The low value in the very beginning arises from the fact that the moving average algorithm has not yet received sufficient measurement values to take the average of an entire set of values, so instead it adds zeros to get the right amount of values.

Using these curves to calculate the radial angular frequency the results are less noisy than figure 6.3b. However the drift due to the

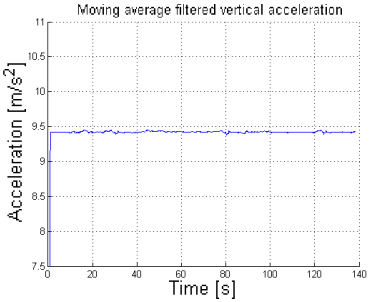

Figure 6.5: Moving average filtered vertical acceleration when opening and closing a door several times.

offset of the tangential acceleration remains. This can be seen in figure 6.6.

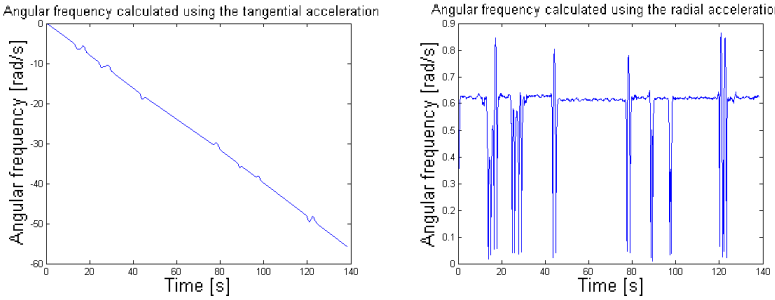

(a) Tangential version

(b) Radial version

Figure 6.6: Angular frequency calculated using moving average filtered acceleration when opening and closing a door several times.

Note that, yet again, the absolute value of the radial version of the angular frequency is shown.

6.1.2.2 Other kinds of filtering

Another kind of filtering is frequency filtering. Studying the spectrogram [1] of the signals, it can be seen that certain frequencies are more prevalent than others. This is shown in figure 6.7. Here a more red

[1] Graph showing the frequency components of a signal at certain time intervals.

colour represents a bigger contribution of that particular frequency and the bluer the colour, the less common that frequency is during the time interval.

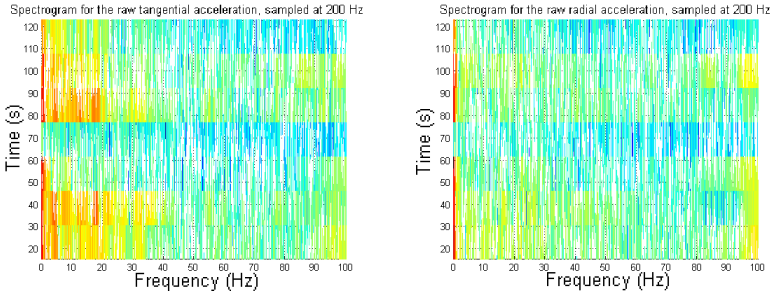

(a) Tangential acceleration

(b) Radial acceleration

Figure 6.7: Spectrogram of the accelerations for the moving sequence of the door.

As can be seen the majority of the signal is very low in frequency. Apart from that, the frequencies appear to be spread out evenly across the spectrum. This indicates that this represent white noise. To get rid of said white noise a low-pass filter could then be applied.

By applying a first degree low-pass Butterworth[2] filter in the frequency plane the high frequency contribution to the signal can be removed, the resulting filtered values are shown in figure 6.8.

Here most of the noise is removed, however some still remains, especially where there have been large peaks in the raw data. This could be due to the fact that the higher frequencies are gradually dampened in the Butterworth filter design and thus still contribute, albeit to a smaller extent. Using the filter described in section 5.2.3, one can efficiently cut off the high frequencies instead of just damping them. The result is shown in figure 6.9.

Even more of the noise is now removed but some of the white noise still remains, which is expected since it is spread out all over the frequency spectra. Should one try to remove this as well the sharpness of the peaks will be affected, since they also require higher frequencies in comparison.

[2]Filter that gradually dampens frequencies after the cut-off frequency, thus no abrupt disappearance of frequencies.

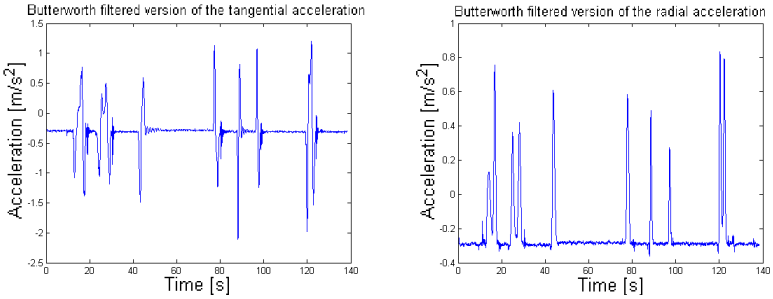

(a) Tangential acceleration (b) Radial acceleration

Figure 6.8: 1st degree low-pass Butterworth filtered acceleration when opening and closing a door several times.

One kind of filtering mentioned earlier, in section 5.2.3, is the wavelet filtering algorithm, here using the Haar wavelet of level 5, meaning 5 times decomposition, the results are shown in figure 6.10.

This filtering quite well preserves the height of the peaks, which might not always be the case with a too aggressive moving average filtering. However some white noise still remains. Considering the extra computational power needed for this kind of filtering, compared with moving average filtering, it is simply not worth the effort.

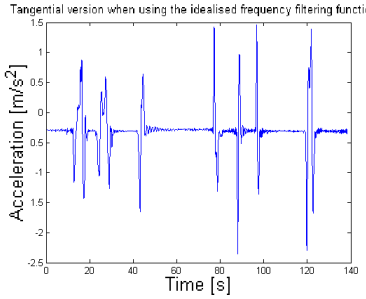

(a) Tangential acceleration

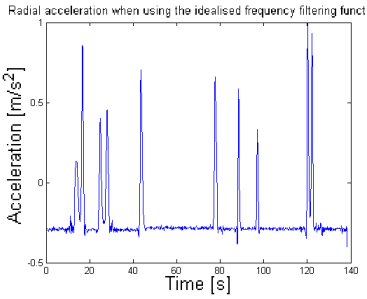

(b) Radial acceleration

Figure 6.9: Idealised frequency filtered acceleration when opening and closing a door several times.

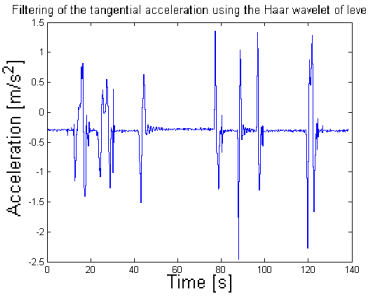

(a) Tangential acceleration

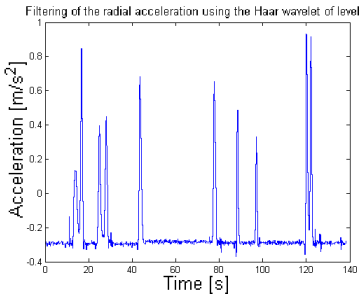

(b) Radial acceleration

Figure 6.10: Wavelet filtered acceleration when opening and closing a door several times.

6.1.3 Correcting rotation

To correct for the rotation of the device firstly the roll and pitch angle need to be found. Studying the same set of data as filtered in section 6.1.2.1 the average value for the stationary z-axis is 9.4215 m/s^2 and the average value for the y-axis is -0.2986 m/s^2. Using eq. (4.7) the roll angle, ϕ, is thus determined to be $-1.76°$. Combining this with eq. (4.8) the pitch angle, θ, can then be determined to be $1.81°$.

Using the matrices of rotation of eq. (4.1) and eq. (4.2), the accelerometer values can then be corrected. The x- and y-axis values are shown before and after derotation in figure 6.11.

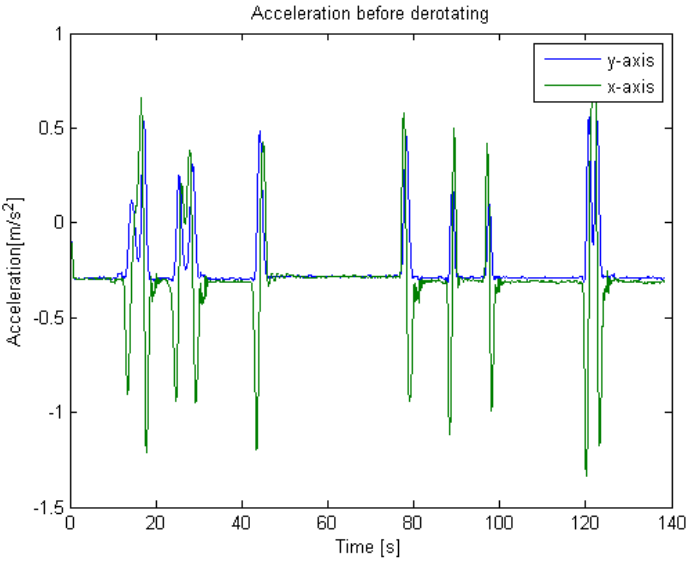

(a) Rotated acceleration

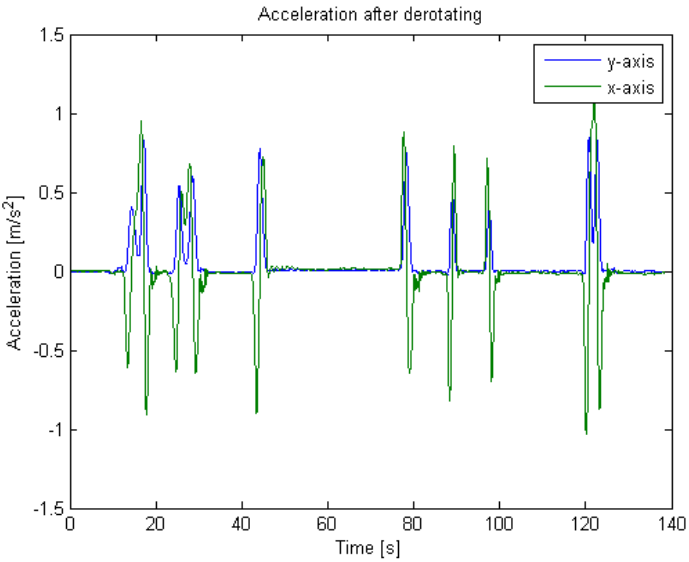

(b) Derotated acceleration

Figure 6.11: Difference between the rotated and derotated acceleration values when opening and closing a door several times.

What should be noted here is that no more calibration of the scale factors has been performed, except the factory calibration, causing the z-axis, even after derotating, to stay at 9.41 m/s^2 instead of 9.82 m/s^2. This however is a scale factor error and therefore, as can be seen, the measurement values correctly go to 0 when no acceleration is present.

Using these derotated values to calculate the angular frequency gives the curves shown in figure 6.12.

Here the absolute value of the radial version of the angular frequency is shown again.

What can also be seen is that the tangential version of the angular frequency drifts away from zero between the peaks. This is due to very small deviations from 0 m/s^2 for the tangential acceleration, which increase during integration. These small deviations can be partially due to the device not being properly fastened on the door, since it has been attached using adhesive compound. When properly attached

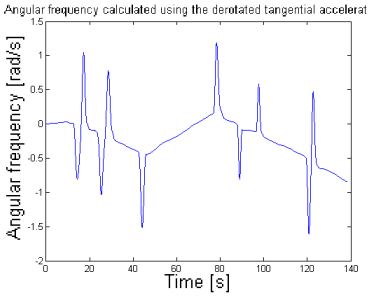

(a) Tangential version

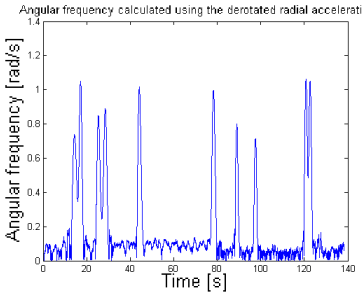

(b) Radial version

Figure 6.12: Angular frequency calculated using derotated acceleration values when opening and closing a door several times.

using nuts and bolts it is likely that these small offsets would decrease.

When calculating the angles from this, according to eq. (3.9), the results are shown in figure 6.13. The radial version of the angular frequency has simply been multiplied with the sign of the tangential version of the angular frequency at a certain time to correct the direction of the angular frequency at said time.

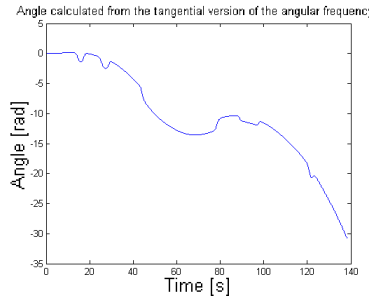

(a) Tangential version

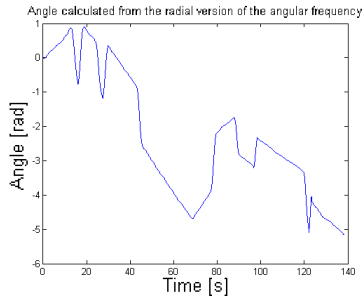

(b) Radial version

Figure 6.13: Angle calculated using the angular frequency values of figure 6.12.

The slight offsets in the angular frequencies cause big deviations in the angular calculations. This is due to the integration procedure, since any error remaining after filtering is also integrated. Firstly the errors from the filtered acceleration propagate to the angular frequency

during integration. Thereafter the errors are yet again integrated when calculating the angle, causing large drifts of the angles.

Note that the angles are expressed in radians, which means that the tangential version ends up at approximately 5 entire rotations of the device and the radial version almost performs a full rotation. The door has during the testing sequence been opened approximately 90 degrees maximum, corresponding to 1.57 radians and a quarter of a rotation.

6.1.4 ZVC

To suppress the small erroneous offsets when there is no acceleration the ZVC algorithm is utilised.

To determine if there is movement the standard deviation is measured for a set of unfiltered values and compared to a threshold. This threshold is determined by measuring the standard deviation of the unfiltered unmoving axis, the z-axis, during a set time. This time has been chosen to be 10 s. For this device this results in a threshold of 0.023 m/s^2.

When using this to detect movement the results are as shown in figure 6.14. Since the accelerometer in this case was turned so that the most sensitive axis was detecting the tangential movement, the threshold was multiplied with 2 for the tangential acceleration and with 1.25 for the radial acceleration. Note that the set of unfiltered values used to calculate the standard deviation correspond to 1 s of data. The different sampling rates are plotted in figure 6.19.

The movement curves here are set to 1 for movement detected and 0 for no movement. When using this to set the acceleration as well as the angular frequency to 0 for no movement detected the angular frequency becomes as shown in figure 6.15. Here the derotated moving average filtered acceleration curves are used for the calculation of the angular frequency when movement is detected.

As can be seen the angular frequency curves, especially for the tangential version, are clearly discontinued at the point that the angular frequency is set to 0. This indicates that some form of error exists in the calculation of the angular frequency. To compensate for this the zero velocity compensation algorithm, according to eq. (5.9) - (5.11) is performed for the tangential version.

For the radial version the modified version of the ZVC algorithm is used, as per eq. (5.14) - (5.15). The resulting curves are shown in

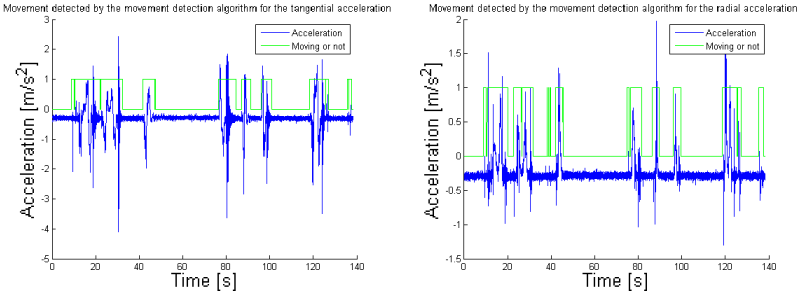

(a) Tangential case (b) Radial case

Figure 6.14: Acceleration used to detect movement as well as the resulting detection of movement, with 1 = movement and 0 = no movement.

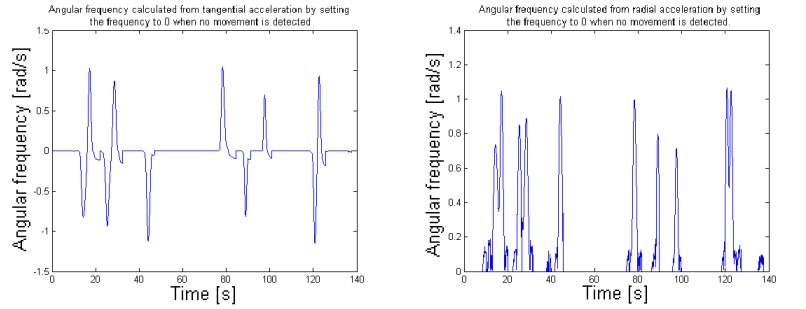

(a) Tangential version (b) Radial version

Figure 6.15: Angular frequency calculated from acceleration that has been set to 0 in the absence of movement. Likewise the angular frequency is set to 0 in the absence of movement.

figure 6.16.

With these corrected curves one can once again try to calculate the angle. Firstly it is however needed to find the sign of the acceleration for the radial version. This is done by multiplying the radial angular frequency values with the sign of the tangential angular frequency. In the cases where the tangential angular frequency is 0 rad/s the multiplicative value is 0. The result is shown in figure 6.17.

As can be seen the first peak starts downwards but the second peak

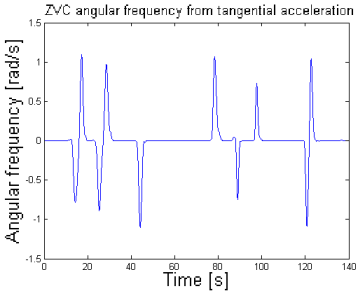

(a) Tangential version

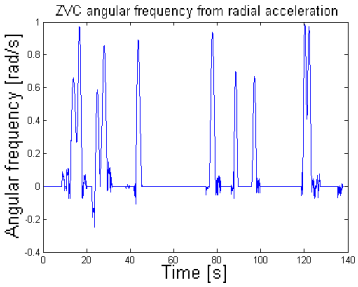

(b) Radial version

Figure 6.16: ZVC of the angular frequency curves of figure 6.15.

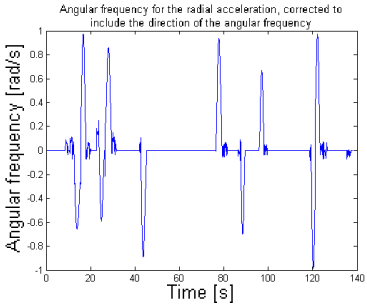

Figure 6.17: ZVC angular frequency for the radial acceleration corrected to include the direction of the angular frequency

has a small positive part before turning negative. This would indicate that one opens the door the ”wrong” direction the second time. This is not true, the door used for testing can only be opened in one direction. The reason for this error is that the removal of bias during ZVC means lowering the entire curve. In this case parts of the curve then became negative, as seen around 20 s in figure 6.16b. Since the radial angular frequency always should be positive this causes an error when multiplying with the direction of the tangential angular frequency.

Furthermore, movement is not always detected at the same time for the two measurement series, radial and tangential acceleration. To combat this in the actual algorithm there is a test to ascertain that the tangential angular frequency is not equal to 0. In those cases the radial angular frequency is assumed to have the same value as the previous

value of the angular frequency.

Using this, the angles are then calculated as shown in figure 6.18.

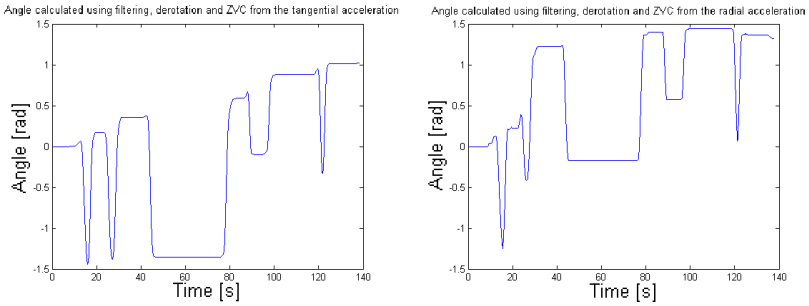

(a) Tangential version

(b) Radial version

Figure 6.18: Resulting angles for the filtered, derotated and ZVC acceleration values.

As can be seen the algorithm is quite good at predicting when there is movement, but it is subjected to quite large drift in the angle. Already during this measurement, of 140 s, corresponding to roughly 2.5 minutes, the algorithm has drifted around 1 radian, being almost as much as the door is opened. Therefore some form of correction is required to reset the angular calculations.

6.1.5 Adaptation of sampling rate for power savings

To save power the adaptation of the sampling rate is important. Having too high a sampling rate will consume unnecessary power, but having too low sampling rate will not necessarily detect the movement of the door. Therefore tests have been performed to observe the effects of different sampling rates. Since the detection of movement using the ZVC will depend on the standard deviation, this has also been plotted, as seen in figure 6.19. Here the standard deviation is calculated for 1 second of samples at the time, creating a so called sampling window of 1 s.

As can be seen, too low a frequency does not accurately detect low acceleration movement, as the standard deviation of this is considerably lower than the large peaks. These peaks arise from the vibrations due to friction against the door frame when closing the door. As the sampling rate increase the low accelerations become clearer, however

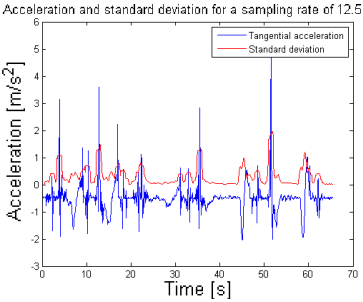

(a) 12.5 Hz

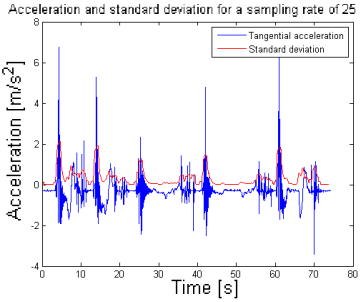

(b) 25 Hz

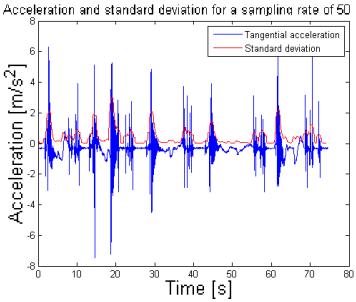

(c) 50 Hz

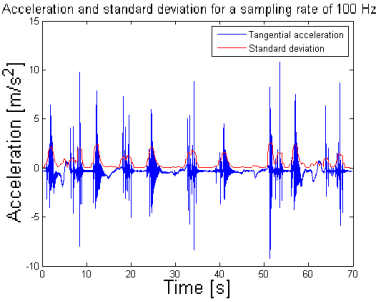

(d) 100 Hz

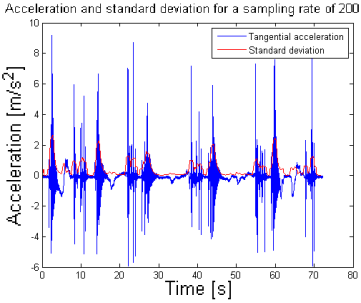

(e) 200 Hz

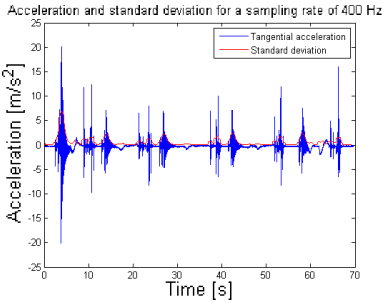

(f) 400 Hz

Figure 6.19: Tangential acceleration and standard deviation for different sampling rates.

so does the vibrations due to friction. For 400 Hz sampling rate the standard deviation of the actual acceleration is very low compared to the friction. This is not only a problem as this friction indicates that

the door is in contact with the door frame, either leaving it (opening the door) or reaching it (closing the door). However, in the event that one manages to open the door without giving rise to these vibrations (perhaps very slowly) it would not be detectable.

One could therefore imagine filtering this signal, using moving average filtering, before calculating the standard deviation, as shown in figure 6.20.

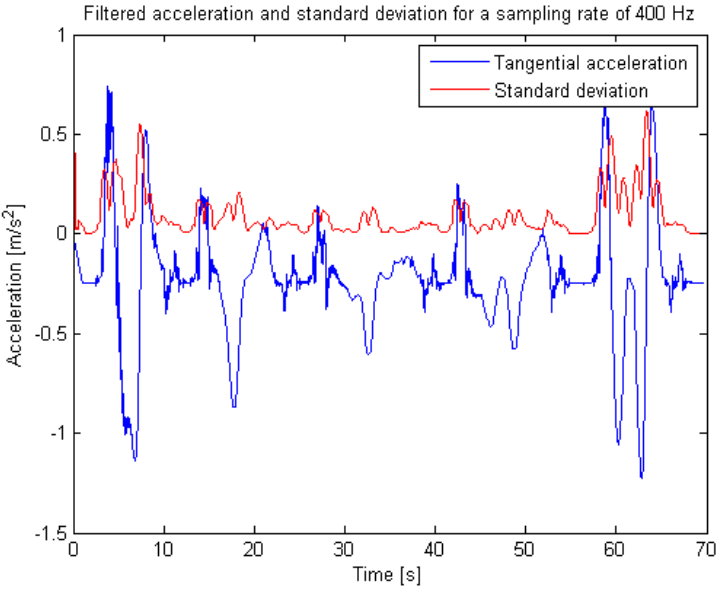

Figure 6.20: Filtered 400 Hz acceleration and standard deviation

Here the acceleration is definitely more apparent, however the standard deviation is still not much larger than the noise level. Therefore the best sampling rate might not be the absolute highest, even ignoring the power saving argument. The sampling rate used for the other measurements is 200 Hz.

6.2 Magnetometer

6.2.1 Raw data

An example of the raw data of a magnetometer when opening and closing the door can be seen in figure 6.21. This data is from the same series of measurements as those of the accelerometer data of section 6.1.

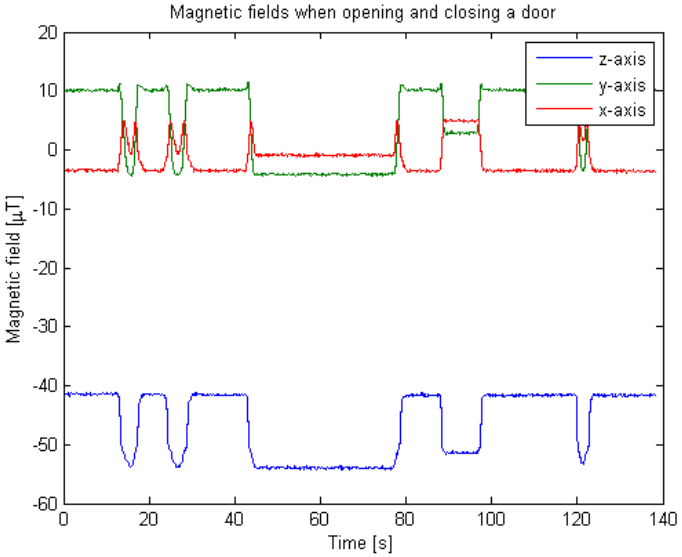

Figure 6.21: The raw magnetometer data when opening and closing the door.

Even though no filtering is applied the curves appear to be quite well behaved. To save computer power no further filtering is therefore performed. What can also be noticed is that the z-axis, not subjected to any rotation, still changes size even though the vertical component of the geomagnetic field should remain the same. This could therefore be understood as a consequence of the varying magnetic fields in the surroundings when opening a door.

For a more complete view these magnetometer values can be plotted in 3 dimension, as shown in figure 6.22.

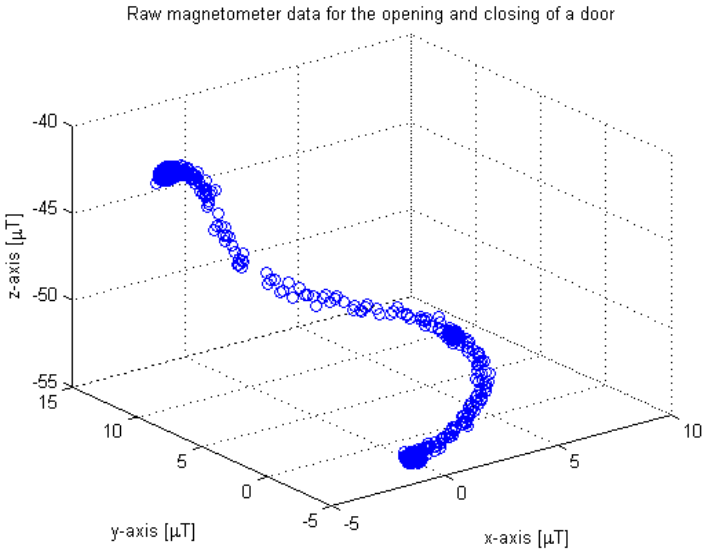

Figure 6.22: The raw magnetometer data in 3 dimension

6.2.2 Correcting rotation

Since these magnetometer values were obtained simultaneously with the accelerometer values of section 6.1, these are used to determine the pitch and roll angles, according to eq. (4.7) and eq. (4.8). The roll angle, ϕ, is thus determined to be $-1.76°$ and the pitch angle, θ, to $1.81°$.

Using eq. (4.1) and eq. (4.2), together with these angles the measurement values can then be derotated, resulting in figure 6.23.

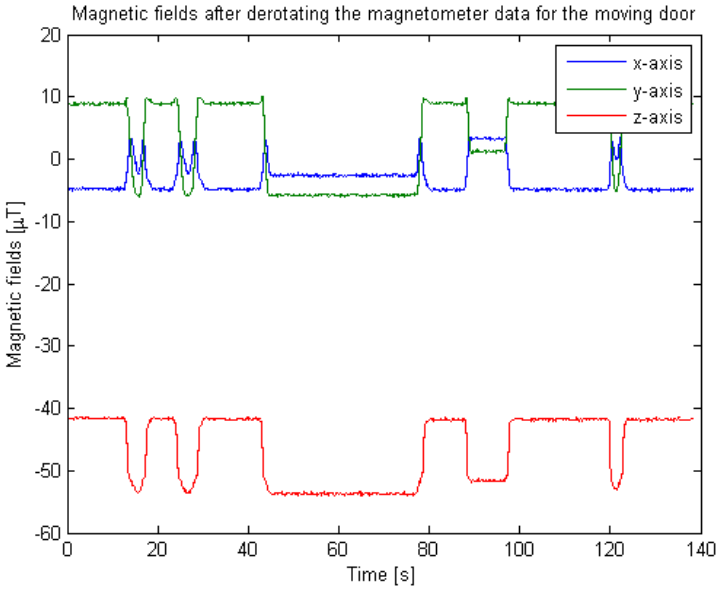

Figure 6.23: The rotated magnetometer data for the opening of the door

6.2.3 Correcting for hard- and soft-iron effects

To be able to compensate for the hard-and soft-iron effects the magnetometer is rotated in as many directions as possible. The raw data for this can be seen in figure 6.24.

This can be plotted in 3 dimensions, as shown in figure 6.25.

What is most apparent here is that the measurement data is not placed on the surface of the sphere representing the geomagnetic field. This is a clear sign that the measurements are affected by either soft-iron effects or scale-factors or both.

Calculating the hard-iron effects for this particular set of measurements values using eq. (A.3) - (A.9), one obtains the vector $V = \begin{pmatrix} -6.5359 \\ 1.5115 \\ -9.4932 \end{pmatrix} \mu T$.

The values of the initial calibration can be derotated by finding the pitch and roll angles for every point, which enables finding the

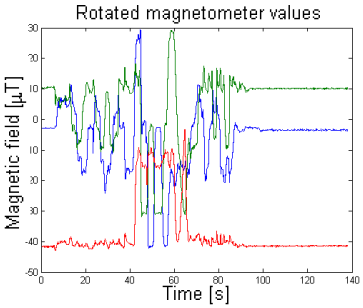

Figure 6.24: The calibration rotational magnetometer data

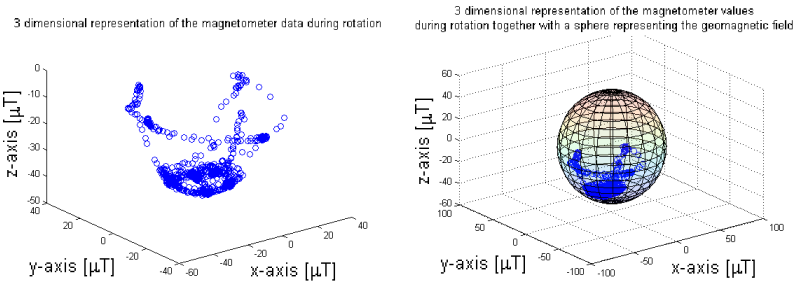

(a) (b)

Figure 6.25: (a) Magnetometer data during the rotation for the calibration, in 3 dimensions. (b) Same data plotted in a sphere with radius equal to the geomagnetic field.

rotation matrices for every moment.

Furthermore the soft iron effects and the scale factors can be found using eq. (A.12) - (A.14), for every moment. The resulting derotated and hard-and soft-iron compensated magnetometer data is shown in figure 6.26.

Using these methods to correct the magnetometer data, the resulting curves for the moving door are shown in figure 6.27.

As can be seen the vertical component, measured by the z-axis, now remains constant. However, the value is slightly too large, which indicates that the soft-iron compensation was not completely successful. Since this represents the vertical component of the geomagnetic field it should correspond to 47 μT without external disturbances. The

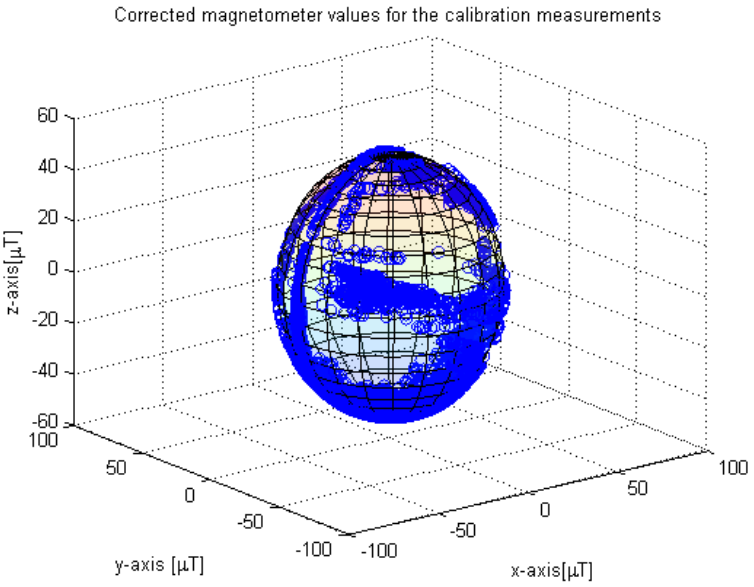

Figure 6.26: The corrected calibration rotational magnetometer data

fact that it does not is likely due to the algorithm being confused by too large magnetic fields in the surroundings. This can also be represented in 3 dimensions, as shown in figure 6.28.

Notice how the corrected magnetometer values are placed on the sphere with radius equal to the geomagnetic field. Zooming in on these magnetometer values, as per figure 6.29, it is yet again apparent that the correction is not completely successful. Here the theoretically calculated values for the opening and closing of a door only affected by the geomagnetic field are also plotted, in green.

Using these values to calculate the yaw angle, according to eq. (3.12) and (4.14) the resulting angle can be plotted as in figure 6.30.

As can be seen the angle is slightly larger than the approximately 1.5 radians corresponding to a quarter of a circle.

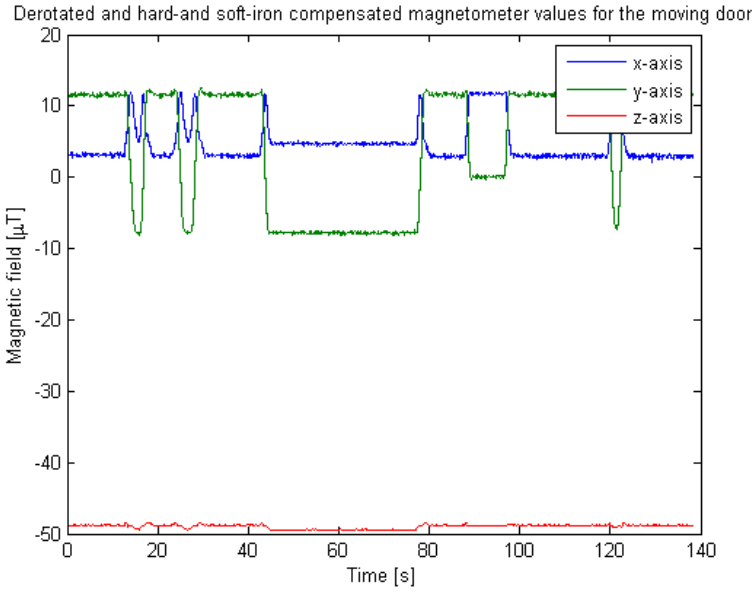

Figure 6.27: The corrected magnetometer data for the moving door

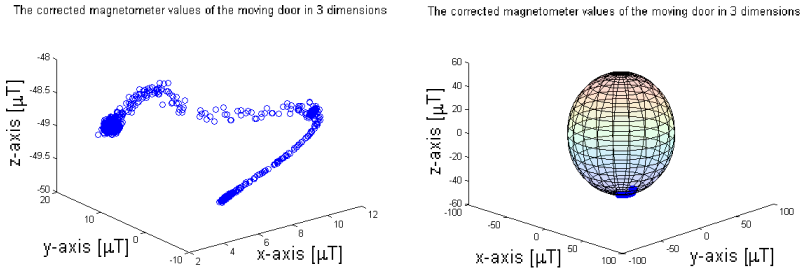

(a) (b)

Figure 6.28: (a) Corrected magnetometer data during the opening and closing of a door, in 3 dimensions. (b) Same data plotted in a sphere with radius equal to the geomagnetic field

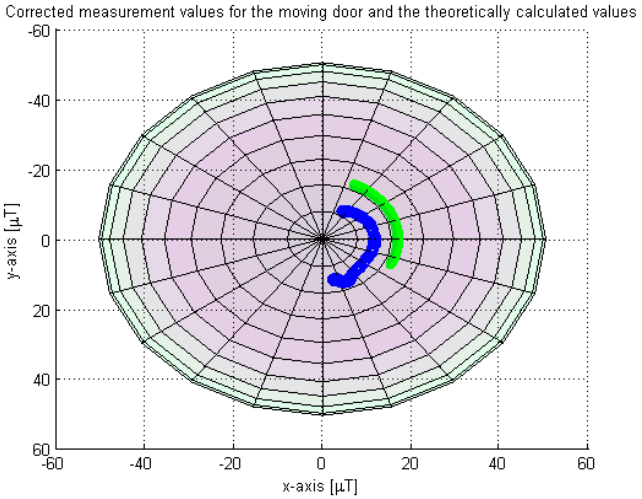

Figure 6.29: The corrected magnetometer data in x- and y-direction, represented by the blue curve, as well as the theoretically calculated values for the opening and closing of a door, represented by the green values. It is all plotted on a sphere corresponding to the geomagnetic field.

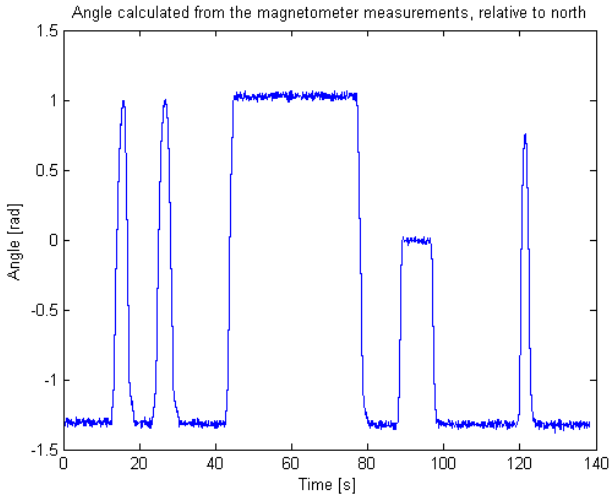

Figure 6.30: Angle relative to north calculated from the corrected and derotated magnetometer values

6.2.4 Adaptation of the calibration for low power operation

The previous calibration of the magnetometer values requires computer power capable of performing inverse matrix transformations and finding eigenvalues and eigenvectors. In the cases where this kind of computer power is lacking the simplified calibration methods of section 5.1.1 and 5.1.2 are used. However, as can be seen in figure 6.25a, not all possible directions were successfully rotated to during calibration. This means that the hard-iron effects and the soft-iron effects will not correspond to those determined using a more complex function.

Using eq. (5.1), the hard iron effects are determined to be $V = \begin{pmatrix} -6.4270 \\ -1.3489 \\ -23.0499 \end{pmatrix} \mu T$

Comparing this with the previously calculated values for the more complex function one can see that the x-values are quite good, most likely owing to the fact that an entire rotation was performed in x-direction. The z-value however, differs largely between the methods, a result of an incomplete rotation in this direction.

To accurately be able to compare the performance of the complex and the simplified function another series of measurement values are therefore used, which includes a full rotation. The raw data is shown in figure 6.31.

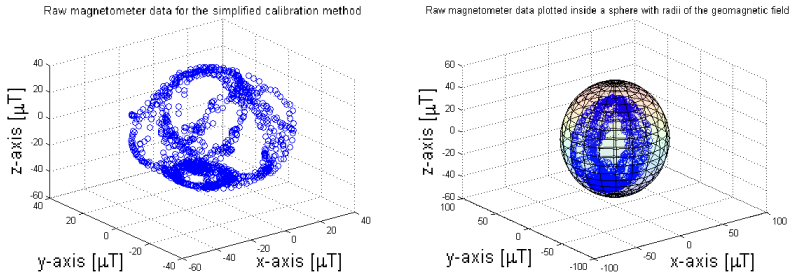

(a) (b)

Figure 6.31: (a) Raw magnetometer data used to compare the performance of the simplified calibration method. (b) Same raw data included in a sphere with radius equal to the geomagnetic field.

Calculating the hard-iron effects for these measurements they are found to be; with the complex calculation method $V = \begin{pmatrix} -5.48 \\ 0.13 \\ -4.51 \end{pmatrix} \mu T$ and with the simplified calculations $V = \begin{pmatrix} -5.83 \\ -0.36 \\ -3.37 \end{pmatrix} \mu T$. As can be seen, the error for this particular set of measurement data, where it is likely that values close to the real extremes have been found, differ around 1 μT.

Calculating the simplified scale factors and soft-iron effects, using eq. (5.2), they are $W^{-1} = \begin{pmatrix} 1.42 \\ 1.53 \\ 1.26 \end{pmatrix}$.

Using this to correct the raw measurement sequence of the moving door of figure 6.32, the result is as shown in figure 6.33.

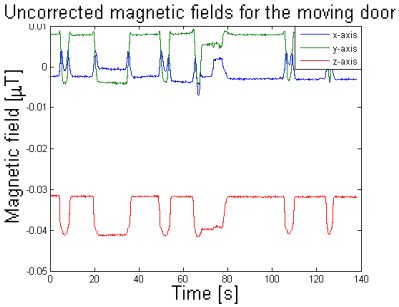

Figure 6.32: Raw magnetometer values for the moving sequence of the door for comparison between the complex and simplified calibration method.

As can be seen the complex function is better at filtering the surrounding fields for the z-axis, but it is not perfect. This can also be plotted on the geomagnetic field sphere for increased clarity, as seen in figure 6.34.

As can be seen none of the functions appear to follow the theoretical values exactly. What is not visible here is that the complex function actually places the values on the geomagnetic field sphere, while the simplified version places them over it (in z-direction). The few measurement values passing through the centre of the sphere are likely

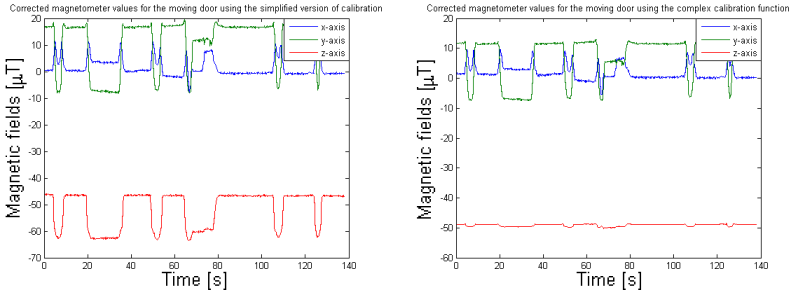

(a) Simplified method (b) Complex method

Figure 6.33: Comparison between the complex and the simplified calibration method of the magnetometer.

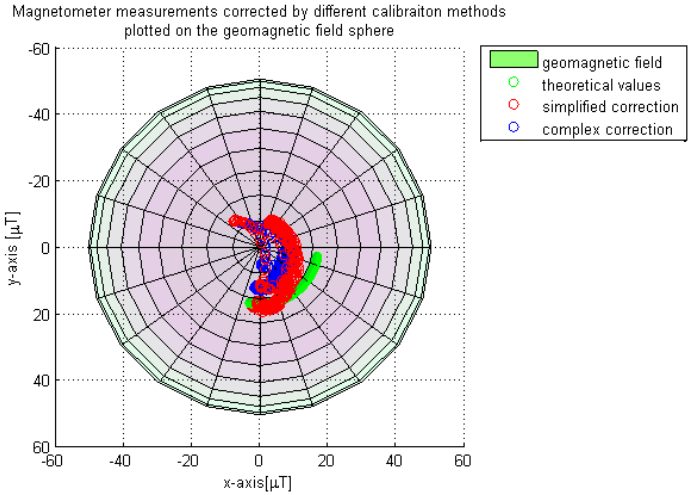

Figure 6.34: Magnetometer values for the moving sequence of the door for comparison between the complex and simplified calibration method plotted on the geomagnetic field sphere. Also the theoretical values for opening a door 90 degrees only affected by the geomagnetic field are included.

due to external rotation of the measuring device at that time, as can be seen more clearly when plotting the angle. This is due to ineffective-

ness of the attachment of the discovery board to the door.

The resulting angles from these 2 calibration methods are shown in figure 6.35.

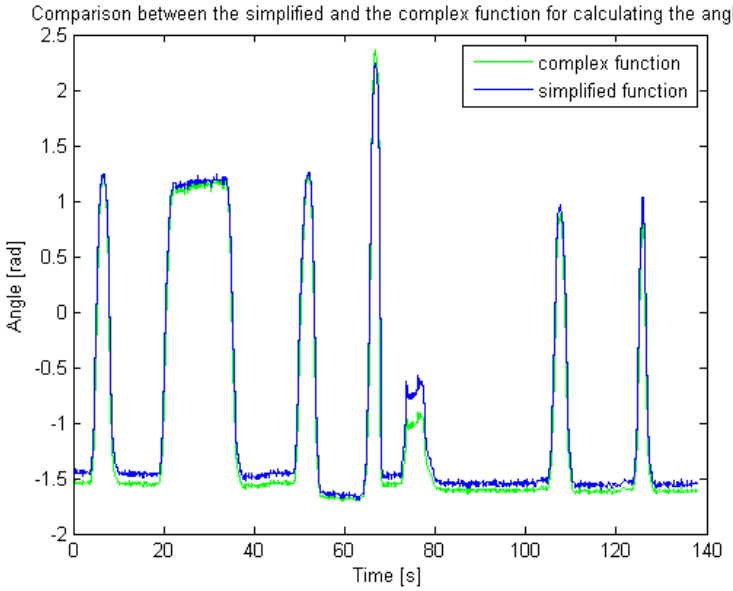

Figure 6.35: Comparison between the angle calculated by the complex calibration function and the simplified calibration function.

This clearly shows that the difference between the two calibration methods is minuscule. It should therefore be possible to use the simplified calibration method to calculate the angle with acceptable accuracy. This, however, is dependant on finding values as close to the extremes as possible during the initial rotational procedure.

The peak at approximately 65 seconds is clearly higher than the others. The value just before is also slightly higher. This is most likely due to a temporary rotation of the device.

The running operation, where the calculation of the angles takes place does not need any memory storage of the earlier results, since no form of moving average filtering or anything similar is performed.

6.2.5 Yaw-scaling

Returning to the angle shown in figure 6.30 it has a promising allure, but the attentive reader will have noticed that the difference in angle between the open and closed door is slightly larger than a quarter of a circle, being approximately 1.5 radians. To compensate this fact it is easiest to scale the calculated angle. This is done by firstly calculating the initial angle, ψ_0. From figure 6.30 it is shown to be -1.31 radians. From the same figure the value of the angle corresponding to the door open a quarter of a circle, ψ_90, corresponding to 1.03 radians.

Using eq. (5.5), one can thus calculate the scaling factor of this angle, with the result being a scaling factor of 0.67. The angle corrected using this method is shown in figure 6.36. Here the angle has also been corrected by subtracting the initial angle, ψ_0, to show the angle of opening and not the deviation from magnetic north.

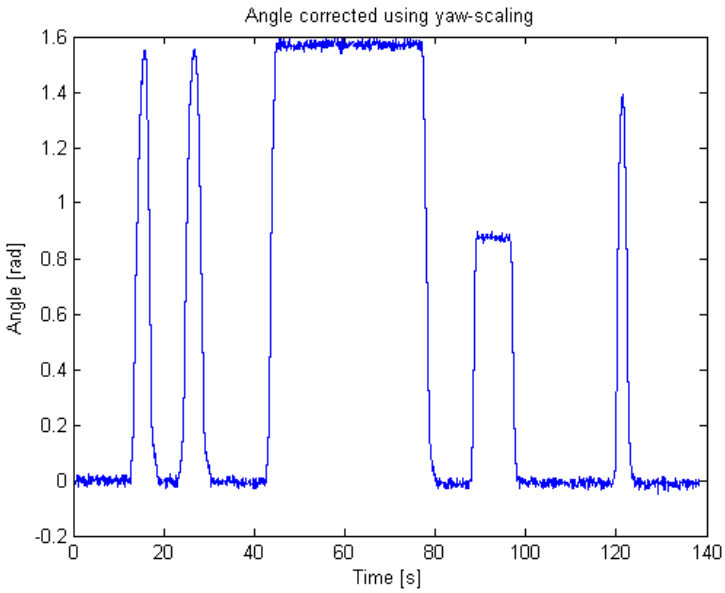

Figure 6.36: Angle from calibrated magnetometer values that has been corrected using yaw-scaling.

The maximum value of this calculated angle can be seen to be around 1.57 radians, which corresponds well to the quarter of a cir-

cle, being $\frac{\Pi}{2}$.

6.3 Components together

6.3.1 Correction without other signals

Knowing that when the door is closed, the angle will be in a local minima, one can compensate for the deviation from 0 at these local minima, as shown in figure 6.37. Here ZVC has been performed as well as correcting for the faulty angle.

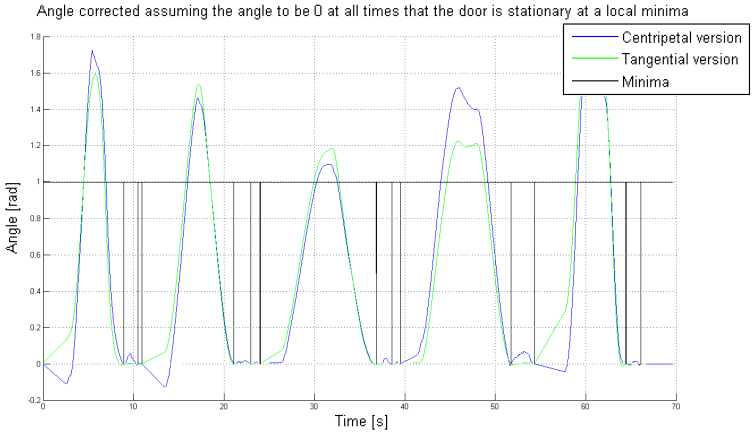

Figure 6.37: Resulting angle when correcting assuming the angle is 0 in the local stationary minima.

The curves appear plausible, however during the generation of the measurement series for this curve the door was partly closed before opening again. This generates a local minima, which this algorithm corrects to correspond to a closed door, which it is in fact not. Thus one can get reasonable values, but fail to detect when the door is not closed.

6.3.2 Correction using magnet contact

To illustrate the possibility of compensating for an erroneous angle, the magnet contact is used to reset the accelerometer angles to 0 when

the door is closed. Using measurement values which have been subjected to ZVC the resulting angles are shown in figure 6.38.

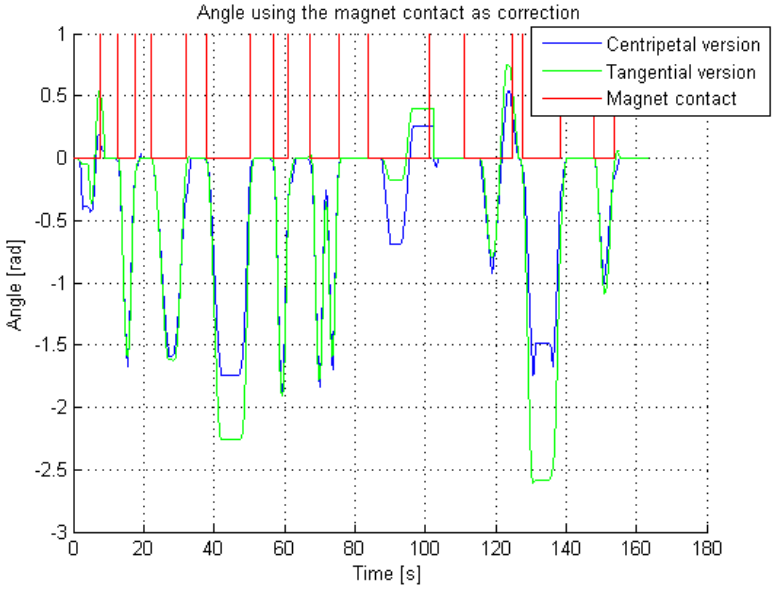

Figure 6.38: Correction of the angle using a magnet contact, as well as the magnet contact signal used for filtering, where 1=open door and 0=close door.

As can be seen no information is given regarding the magnitude of the opening of the door. Therefore the correction is only performed when the magnet contact verifies that the door is closed. This shows that it is possible correct the angle using some kind of more secure signal.

Ideally one might like to correct the angle using the magnetometer and then compare this to the state given by the magnet contact. However as the magnetometer measures magnetic fields and the magnet contact is depending on signals from a magnet, the resulting values from the magnetometer are very inaccurate. Even after correction, the magnetometer series of measurements taken while the discovery kit is in the vicinity of the magnet contact, will be unusable, as shown in figure 6.39.

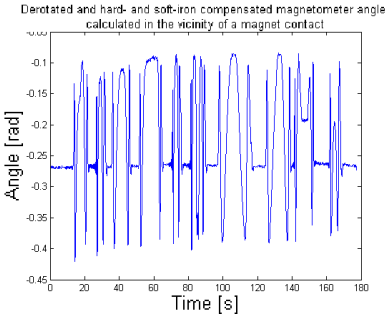

Figure 6.39: Angle calculated after correction of the magnetometer values taken in the vicinity of the magnet contact.

To avoid this, the best option is to separate the magnetometer and the magnet contact considerably to decrease the impact of the magnet on the readings.

What should also be noted is that the magnet is not placed on the PCB for which the hard-iron compensation is performed. Had it been it might have been possible to filter out the magnet as a hard-iron effect, with a moderately spacious PCB and a large range for the magnetic measurements.

6.3.3 Correction using the magnetometer

Connecting the angles calculated by the magnetometer and the accelerometer the first issue is the fact that they might be defined in different directions. This is easily solved by either looking at the absolute values of the angles or redefining the positive direction of one of the angles, by multiplying it by -1.

Assuming that the corrected magnetometer angle is always correct one can use this to compensate for the drift of the accelerometer readings. By simply verifying the angle of the accelerometer at standstill with the angle of the magnetometer, drift is extinguished.

This can either be done, in presence of a large memory, by correcting the past values of the angle, as per eq. (5.17), or simply by setting the accelerometer angle to the value of the magnetometer angle. The different approaches are shown in figure 6.40 and 6.41.

In the first figure mentioned ZVC is firstly performed and then the angle is compensated according to eq. (5.17). As can be seen the result-

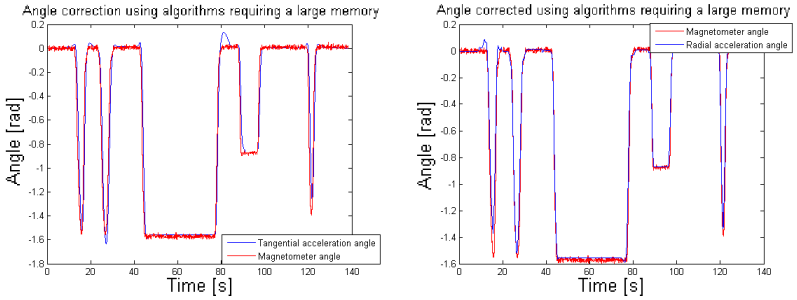

(a) Tangential version

(b) Radial version

Figure 6.40: Correction of the accelerometer calculated angles using large memory, enabling ZVC and correction of the angle.

ing angles are very well corresponding to the magnetometer angle.

In the other figure, figure 6.41, a component with limited memory is envisioned, which has been simulated by looping through the values instead of storing them in a vector. Note that the same series for the magnetometer angle is used, so the red curves of figures 6.40 and 6.41 are the same. This means that the angular frequency can be set to 0 when no movement is detected, but no error compensation can be performed for the previous values, which might lead to incorrect angle calculations. To combat this the movement sensing of the ZVC is utilized and when no movement is detected the angle is simply set to the magnetometer value. This is only performed for the first measurement value of a sequence of stationary position, the following measurement values are derived from said corrected one.

As can be seen the results are relatively well following the magnetometer angle, however there are some local peaks just before the angle is set to the correct value. This should not affect the overall performance, since the values are quickly corrected to correspond with the magnetometer values.

One could envision correcting the accelerometer using the magnetometer angle also during the moving sequence. This will cause problems when sampling the magnetometer at a lower sampling rate. Especially when the door is moving fast this will mean that in periods between two magnetometer measurements the accelerometer will be corrected with an old angle, which is no longer correct. At stationary positions this is not a problem since the angle should not change

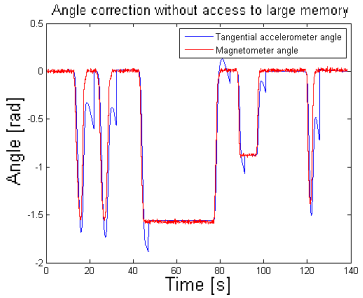

(a) Tangential version

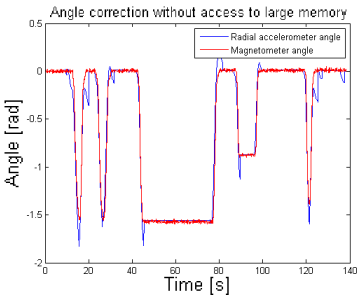

(b) Radial version

Figure 6.41: Correction of the accelerometer calculated angles without access to a large memory.

between samplings.

6.4 Implementation on Cortex-M4 processor architecture

Using the adaptations of the algorithms to a small memory processor, as described in section 5.5, in combination with the adaptation to c-code, as described in appendix B, the algorithm was implemented on the Cortex-M4 processor of the STM32F401 Discovery kit. To decrease the power consumption the magnetometer is sampled at 0.75 Hz and the accelerometer at 100 Hz.

Furthermore no compensation for soft-iron effects is performed as this is deemed to time consuming for an installer and also too power consuming should the more complex function be used. Moreover the soft-iron effects will vary with respect to the position of the door in the room. For a complete correction, calibrations are required for each step of the way of the door. This means either a rotating platform is needed to map the sphere (which will not work since the component is attached) or a lot more work for the installer.

It is assumed that the yaw scaling performed, as described in section 5.1.4, will somewhat compensate for the lack of soft-iron compensation. The reason for this assumption is that the raw x- and y-magnetometer values, without any compensations, are placed on a demi-circle, as seen in figure 6.22. The length of this arc is then compensated by the yaw-scaling to correspond to 90° when the door is opened this amount. The offset of the centre of this circle is taken care of by the hard-iron compensation. This compensation is performed since it is less power consuming and can be calibrated in the factory.

The resulting angles, as calculated by the algorithm on the processor, have been logged to a USB stick. The result is shown in figure 6.42. To evaluate the performance a magnet contact has also been attached to the door, but further away to limit the influence of the magnet on the magnetometer.

As can be seen the accelerometer is reliably signalling when motion is detected and is also accurately noticing stationary positions. The magnetometer on the other hand is reliably noting the angle. The edgy allure of the magnetometer curve is due to the low sampling frequency, resulting in one value per ”step”.

The observant reader might notice the magnetometer sometimes signalling an opening angle of almost 3 radians, which would correspond to nearly 180°. This is incorrect as the door, like for the previous

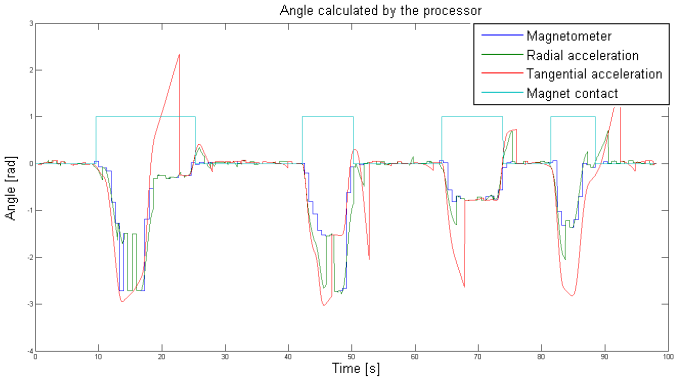

Figure 6.42: Angles calculated by the processor together with output from a magnet contact placed on the same door.

measurement series, has not been opened more than around $90°$.

One explanation for these incorrect angles could be that the arctangent function used in the algorithm is defined between $-\pi$ and $+\pi$. When the real measurements is close to one of the limits it is possible that a slight change in the measured values (from fluctuations of the surrounding magnetic fields or other noise) would cause the angle to pass the boundary and be noted as an angle in another quadrant. With subtraction of the initial yaw angle and yaw-scaling the difference in angle could then appear to be almost $\frac{\pi}{2}$ as seen in the figure. With compensation for soft-iron effects it is likely that these errors would decrease.

The code of this algorithm, without the logging to the USB memory stick, requires 24.9 kB of flash memory and 1.2 kB of RAM memory. This is well within the limits of the ARM Cortex-M4 on the discovery kit used, which has a FLASH memory size of 256 kB and RAM memory size of 64 kB [38].

6.5 Window opening in the plane of gravity

The separate algorithm, developed for a window opened by rotation around a horizontal axis was also tested, using eq. (5.20). The window was here opened a few degrees, less than 20, were it was stopped, be-

fore being closed again. This procedure as repeated a couple of times. The result is shown in figure 6.43.

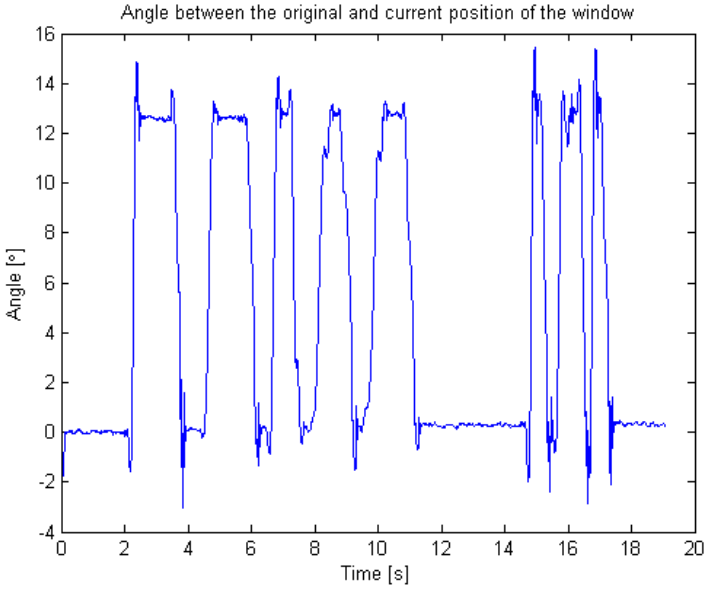

Figure 6.43: Angle of opening for a window that is rotated around the horizontal axis.

No filtering has been used for these calculations, as can be seen in the occasional peaks just before stabilisation of the curve. What can also be seen is that even without this the angle returns to 0 nicely. The window that the test was performed on had a maximum possible angle of opening, to which it was opened several times, a fact that is also well reflected in the curve.

It thus appears that even without filtering it is possible to obtain reliable information on the opening of such a window using only an accelerometer.

7. Discussion

To sum up, it is possible to obtain the angular information using an accelerometer and a magnetometer. An accelerometer in itself is quite good when it only comes to detecting movement, but during a longer measuring sequence it is subjected to drift. To correct this, a magnetometer or some other kind of verification is required.

One could here speculate in simply removing the accelerometer. However, this cannot be done as it is necessary to determine the tilt of the magnetometer. By correcting the calculated accelerometer angle using the magnetometer at stationary positions, the accuracy of the accelerometer angle in the moving door sequence is less important. Since the algorithm is aimed at detecting the closed or open state of the door the exact angle when the door is open is less important. What is important is that it is open.

Correction using the magnetometer assumes that the magnetometer always measures the correct angle which might not be the case. Especially in an indoor environment there are many different sources of magnetic fields, risking a change in the soft-iron effects that might not be possible to compensate for.

Another question that is raised that has not been verified so far is also how it reacts to being placed on a construction of steel, such as a steel door. Other kinds of doors, such as sliding doors also pose a problem using this method. These sliding doors do not turn when opened, therefore the angle does not change. In this case the magnetometer would be unable to detect the opening.

Another concern of utmost importance in field, is the power consumption. The main factor affecting the power consumption is the sampling rates, where the magnetometer is clearly less efficient than the accelerometer. One could envision decreasing both of theses sampling rates, however this also means risking missing a very fast opening of the door, if the person opening and closing the door manages to time it between two sampling occurrences. To combat this one can envision increasing the accelerometer sampling rates, since this component is best at detecting movement and also consumes least power.

However due to the noise, the accelerometer can not discern very low accelerations, as in a very slow opening of a door.

With some calculations it should therefore be possible to find the optimal sampling rates, where the accelerometer catches the quick opening of doors and the magnetometer the slow. However there will always be a trade-off between higher sampling rates, resulting in better accuracy of the algorithm, enabling higher security, and power consumption.

Another possible problem could be that the standard deviations working as thresholds seem to vary slightly from door to door, even when based on measurement values from 10 s of measuring on a certain door. However the problem is usually that the stationary position is not detected, by setting the threshold a bit higher than necessary this would be avoided. The possible opening thus missed could then be detected by the magnetometer.

As noted there are some difficulties in ascertaining the true angle of an accelerometer. Therefore an even more power efficient way of performing the detection of the opening and closing of the door might be to only have the accelerometer detect movement. When it has been detected the magnetometer can be called to verify if the door has moved. This would eliminate the majority of the calculations to be performed for the accelerometer.

To test the performance of the suggested component in field one could envision attaching a magnetometer and an accelerometer to the already existing device of the magnet contact. By placing the actual magnet on the chip it might then be possible to treat the added magnetic field as a hard-iron effect rather than a soft-iron effect. However this means that the hard-iron effects will be very high. To actually be able to still measure the magnetic fields (including the hard iron effects) the range of the magnetometer must be increased, which in turn causes a decrease in the accuracy of the magnetometer. This enables possible false negatives due to noise or other fluctuating fields in the surrounding when using too small an angle as the requirement for closed.

For as accurate values as possible of the hard-iron effects it would be preferable to perform the complex calibration procedure. Technically these do not need to be performed at the place of installation and could therefore be performed in for instance the factory. Here one could attach the device to a computer for the calibration where the power consumption for said calibration would be negligible. The fac-

tory calibration of these effects are also advantageous since it would mean less for the installer to do in field.

During the rotation needed for this one could also take values needed to find the scale factors. The complete soft-iron correction procedure, with the inverse matrix operations, might then be less important, as yaw scaling is still performed.

Another problem with this algorithm is that certain aspects of it would need to be input by the installer, such as the radius of the door. This could also be specified to be, for instance, 75 cm and placing the device 75 cm from the hinges during installation. This would then require having a window option with a considerably smaller radius specified.

Likewise an opening of the door, 90 degrees, is required during installation, which adds tasks to do for the installer. However this might be countered by the fact that only one component, instead of two, needs to be attached, the latter corresponding to the installation of the magnet contact.

Further work that would need to be performed is actually measuring the power consumption, as the assumed higher power consumptions might not actually be that big. Perhaps the usage of the more complex function does not actually draw that much power and can be used without problems.

8. Conclusion

To sum up it is possible to use the combination of an accelerometer and a magnetometer investigated in this report to determine the opening angle of a door or window. Also the implementation of the algorithm on Cortex-M4 processor architecture is possible. However to generalise this method to work on all kinds of doors more work is needed. Even then it is unlikely to work on sliding doors.

The power consumption of the measurement components in itself is in the range of μA and can be further decreased by controlling the sampling rates. Also the power consumption of the algorithm can be decreased by choosing less complex computational methods. However, this way of limiting the power consumption also impairs the reliability and accuracy of the device. Hence there exists a trade-off between power consumption and performance that should be optimised in order to find the most beneficial configuration.

In comparison with the magnet contact the big advantage of the method described herein is the possibility to detect tampering and to deal with this accordingly. For instance the accelerometer could be used to determine if the door is moving during tampering attempts.

Simply put: the algorithm works, but more work is needed.

Appendices

A. Finding hard- and soft-iron effects

As discussed in section 3.2.3 the hard and soft iron effects need to be found. This can be done using the following approach as outlined in [24].

The magnetic values B_p are the sum of V and the actual values. Supposing there are no soft-iron effects the hard-iron effects can thus be calculated as follows. The entire derivation of the way to obtain the hard iron effects are found in [24].

$$(B_p - V)^T (B_p - V) = B^2 \tag{A.1}$$

$$V = \begin{pmatrix} V_x \\ V_y \\ V_z \end{pmatrix} \qquad B_p = \begin{pmatrix} B_{px} \\ B_{py} \\ B_{pz} \end{pmatrix}$$

where B indicates the total magnetic field. The residual error, r, for a certain set of measurement values are then

$$r = B_p^T B_p - 2B_p^T V + V^T V - B^2$$
$$r = B_{px}^2 + B_{py}^2 + B_{pz}^2 - 2B_{px}V_x - 2B_{py}V_y - 2B_{pz}V_z + V_x^2 + V_y^2 + V_z^2$$

which can be rewritten as

$$r = \left(B_{px}^2 + B_{py}^2 + B_{pz}^2\right) - \begin{pmatrix} B_{px} \\ B_{py} \\ B_{pz} \\ 1 \end{pmatrix}^T \begin{pmatrix} 2V_x \\ 2V_y \\ 2V_z \\ B^2 - V_x^2 - V_y^2 - V_z^2 \end{pmatrix} \tag{A.2}$$

By taking a number of different measurements, n, the new variables X, Y and β can be introduced.

$$Y = \begin{pmatrix} B_{px}[1]^2 + B_{py}[1]^2 + B_{pz}[1]^2 \\ \vdots \\ B_{px}[n]^2 + B_{py}[n]^2 + B_{pz}[n]^2 \end{pmatrix} \tag{A.3}$$

$$X = \begin{pmatrix} B_{px}[1] & B_{py}[1] & B_{pz}[1] & 1 \\ \vdots & & & \\ B_{px}[n] & B_{py}[n] & B_{pz}[n] & 1 \end{pmatrix} \tag{A.4}$$

$$\beta = \begin{pmatrix} \beta_1 \\ \beta_2 \\ \beta_3 \\ \beta_4 \end{pmatrix} = \begin{pmatrix} 2V_x \\ 2V_y \\ 2V_z \\ B^2 - V_x^2 - V_y^2 - V_z^2 \end{pmatrix} \tag{A.5}$$

Note that no matter the number of measurements, the size of β remains unaffected as the hard-iron effects are constant offsets arising from the PCB. The total magnetic field is likewise constant since we assume that there are no soft-iron effects. Inserting these formulas into eq. (A.2) one obtains a vector of the residual errors, **r**, which can now be expressed as

$$\mathbf{r} = Y - X\beta \tag{A.6}$$

From this a new function, the performance function, can be defined as the square of the residual error.

$$P = r^T r (Y - X\beta)^T (Y - X\beta) \tag{A.7}$$

which is minimised for

$$\begin{aligned} Y &= X\beta \\ \beta &= (X^T X)^{-1} X^T Y \end{aligned} \tag{A.8}$$

which can be shown in a more proper mathematical fashion as well. Said function is often known as ”the normal equation for least squares optimisation”. Thus beta can be determined and from that the hard-iron offsets, V, according to eq. (A.5), being the first three values of β divided by two.

$$V = \frac{1}{2}\begin{pmatrix} \beta_1 \\ \beta_2 \\ \beta_3 \end{pmatrix} \tag{A.9}$$

Onto the soft iron effects. In reality there will probably exist soft-iron effects as well that need to be taken into account, arising from induced magnetic fields. The sphere mentioned earlier will, due to these effects, appear as an ellipsoid. Luckily soft-iron effects can be calculated with the approach in [24] and compensated for.

Modelling the soft-iron effects as a matrix, W^{-1} of rank 3, the measured values (supposing no misalignment), B_p, can be expressed as

$$B_p = WB + V \tag{A.10}$$

the square of the absolute value of the readings can thus be expressed as

$$W^{-1}(B_p - V)^T W^{-1}(B_p - V) = B^2 \tag{A.11}$$

which has clear similarities to the general equation for an ellipsoid

$$(R - R_0)^T A(R - R_0) = C \tag{A.12}$$

with R being a three-dimensional vector of measurement values, R_0 being a three-dimensional offset vector, A a symmetric matrix and C a constant. By posing $X = R - R_0$ for eq. (A.12), it can be solved for A.

$$\begin{aligned} (X)^T A(X) &= C \\ (XX^T)A(XX^T) &= XCX^T \\ (XX^T)^{-1}(XX^T)A(XX^T)(XX^T)^{-1} &= (XX^T)^{-1}XCX^T(XX^T)^{-1} \\ A &= (XX^T)^{-1}XCX^T(XX^T)^{-1} \end{aligned}$$

By comparing eq. (A.11) with eq. (A.12) it can be seen that

$$\begin{aligned} A &= {W^{-1}}^T W^{-1} \\ sqrt(A) &= W^{-1} \end{aligned} \tag{A.13}$$

which enables the calculation of the soft-iron effects. It can be argued that the constraint that W^{-1} should be symmetric can be imposed ([24]). This means that the eigenvectors of W^{-1}, v, are the same as those of A and that the eigenvalues of A, λ, are the square of the eigenvalues of W^{-1}.

$$\begin{aligned} Av &= \lambda v \\ W^{-1}v &= \sqrt{\lambda}v \\ W^{-1}vv^T &= \sqrt{\lambda}vv^T \\ W^{-1} &= v\sqrt{\lambda}v^T \end{aligned} \tag{A.14}$$

Using all these formulas the corrected measurement values, B_c, can finally be calculated as

$$B_c = W^{-1}(B_p - V) \tag{A.15}$$

This permits the calculation of the angle of interest, being the angle between the initial vector and the vector at the time of interest in the plane orthogonal to gravity. Since the z-axis by convention is pointed in the direction of gravity, the angle between the x-axis and magnetic north, ψ_{mag} can be calculated as

$$\psi_{mag} = tan^{-1}\left(\frac{-B_{cy}}{B_{cx}}\right) \tag{A.16}$$

B. Implementing the algorithm in C-code

Since this code was developed in Matlab, on a PC, with slightly more computer power than the little Cortex-M4 processor on the chip used to implement the algorithm. This causes some need for changes. Some of which are described below. Luckily Matlab also has a built-in C-code converter which simplifies the life of anyone trying to implement Matlab programs on small processors.

- **Standard deviation** Firstly such simple things as finding the standard deviation, needed to determine if there is movement, requires a number of values to perform the operation described by eq. (5.16). The amount of measurement points used for this can be determined by the user and depends on which "resolution" is preferred. In the implementation of this algorithm the number of points used correspond to sampling during 1.3 seconds of accelerometer data. The reason for this odd number is that the magnetometer is sampling with a frequency of 0.75 Hz, corresponding to 1.3 seconds between the sampling events. This means that the vector of accelerometer data contains 133*3 samples. To calculate the mean of this vector and the mean of the square of the vector for every new value will require quite many operations. Therefore the sum of all the values in the vector is stored in one variable, sum as well as the sum of the square of all the values, $sum2$. The standard deviation can the be calculated as

$$\sigma = \sqrt{\frac{sum2}{133} - \frac{sum * sum}{133^2}} \tag{B.1}$$

  Every time a new value is read the value of these two variables are changed. For sum the value is simply added while the oldest value in the vector is subtracted. Likewise for $sum2$ the square

of the value is added while the square of the oldest value in the vector is subtracted.

- **Matrix adaptation and vector multiplications** Matlab is, to a large extent, very encouraging of vector- and matrix-operations. For instance the multiplication of two vectors into a matrix requires a single operation (for the person writing the script). However C does not support matrices and no vector operations (such as multiplication are implemented). To simulate a matrix an array of the same length as the number of elements in the matrix is used. Instead of placing the rows of the matrix under each other they are simply placed after one another.

  Vector multiplication is simply achieved by looping through the vectors and adding the products of each step in the loop. Matrix multiplication on the other hand requires nested loops. Here one loop loops through the current row and the other loop loops through the rows. The latter is done by incrementing the index with a factor corresponding to the length of the row in real matrix-form.

- **Removing oldest from array** Another structure that is not implemented in C is a queue, which would be perfect for the purpose of storing the accelerometer values used to calculate the standard deviation among other things. However, since only an array is available this is used instead. To keep track of which value is the oldest a simple variable is used, that counts the number of values added to the vector. As this counter becomes greater than the size of the array the size of the array is simply subtracted from the counter, using the % operation. To remove the oldest value from the array and add a new one the value at place counter is simply replaced by the new value.

C. Effects of algorithm operations on measurement values

To simplify the view of the effect that every step of the algorithm has on the measurement values the following image series aims to show images representing the operations of the algorithm on the measurement values.

C.1 Accelerometer

Tangential acceleration **Radial acceleration**

Raw data

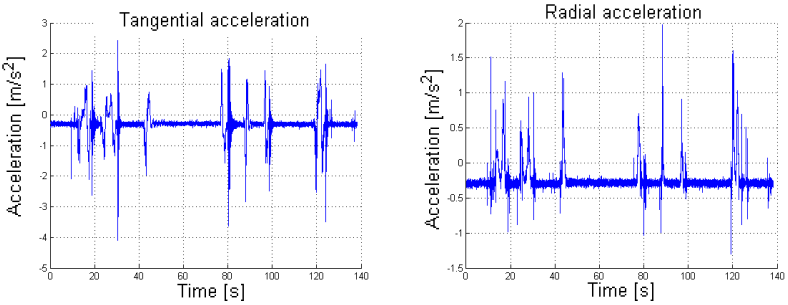

↓ Moving average filtering

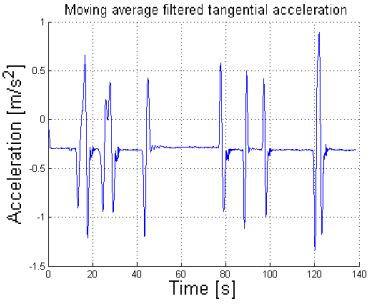

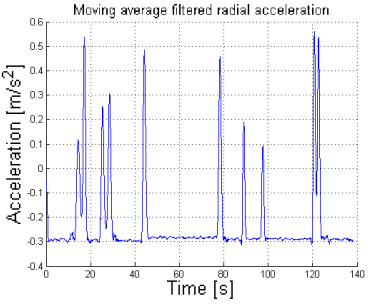

↓ Derotation

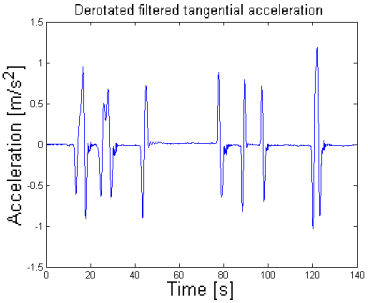

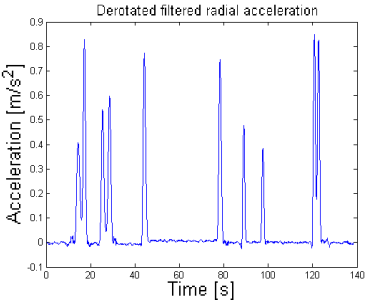

↓ Angular frequency

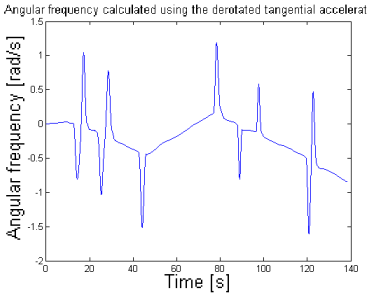

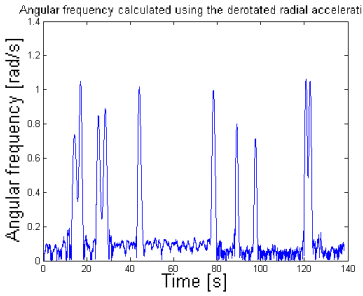

↓ ZVC

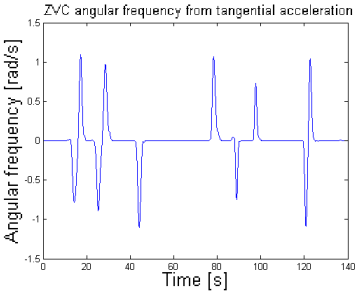

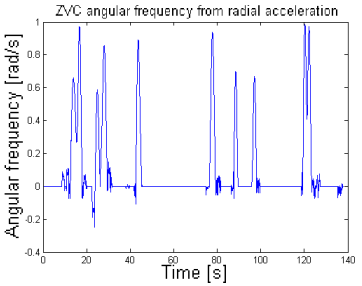

↓ Correcting direction

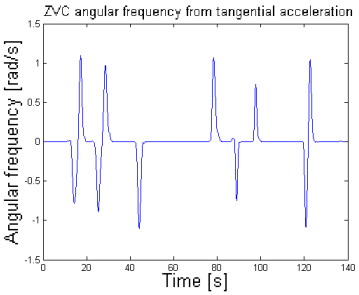

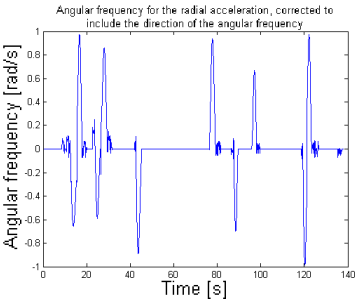

↓ Angle

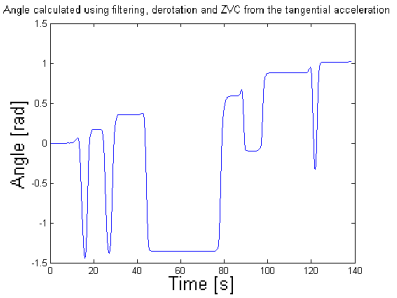

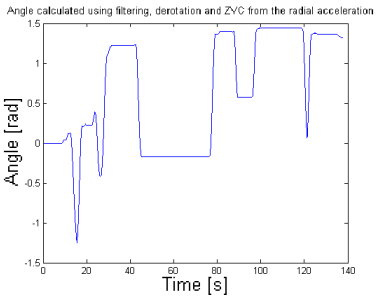

↓ Correcting with magnetometer

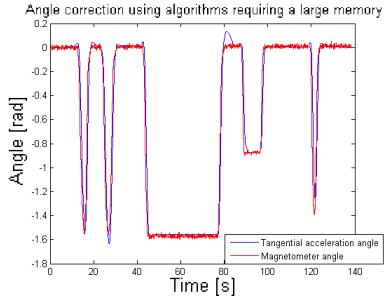

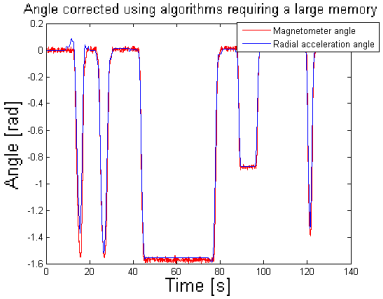

C.2 Magnetometer

For the purpose of being able to compare the more complex and the simplified way of calculating the hard- and soft-iron effects another series of measurements are used than in section C.1.

Complex function	**Simplified function**
Raw data	

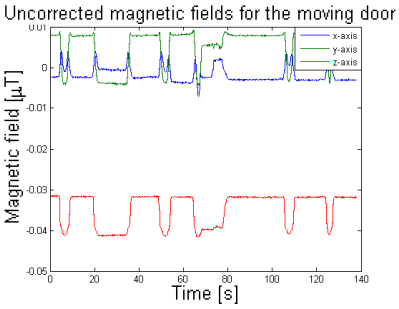

↓ Derotation

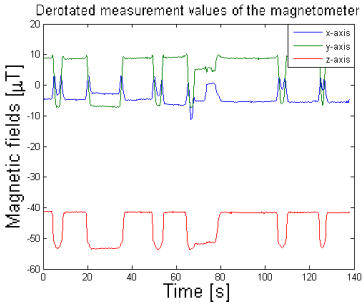

↓ Compensating hard-iron effects

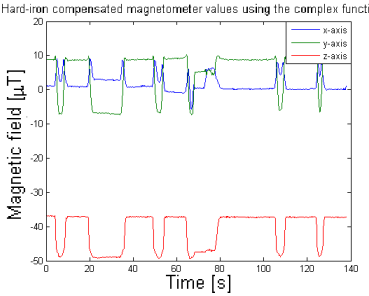

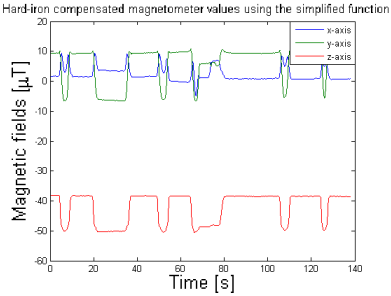

↓ Compensating soft-iron effects

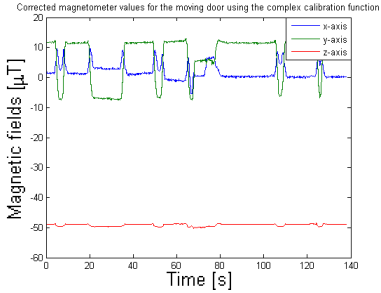

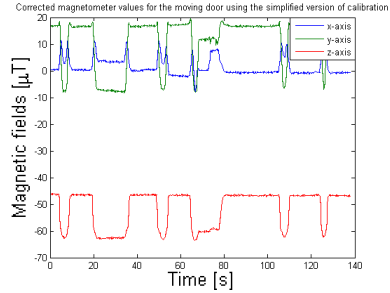

↓ Angle

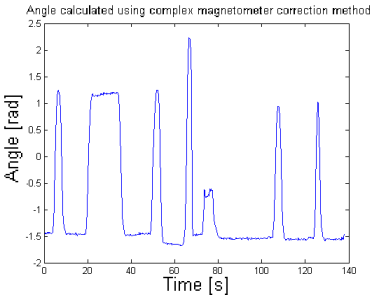
Angle calculated using complex magnetometer correction method
Angle [rad]
Time [s]

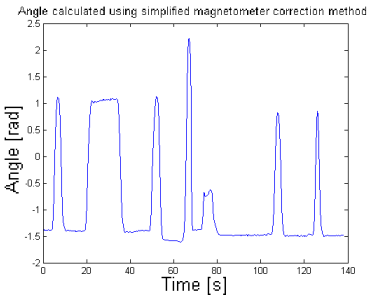
Angle calculated using simplified magnetometer correction method
Angle [rad]
Time [s]

Bibliography

[1] S. Sukkarieh, P. Gibbens, B. Grocholsky, K. Willis, H. F. Durrant-Whyte, "A low-cost, redundant intertial measurement unit for unmanned air vehicles",textitThe International Journal of Robotics Research, vol. 19, no. 11, pp. 1089-1103, 2000

[2] M. Frank, "Positioning refinement algorithm", US Patent no. US 6,292,751 B1, Sep. 18 2001

[3] Z. Zhou, Z. Wang and L. Lin, "Microsystems and Nanotechnology", Springer, pp. 654-694, 2012

[4] "MEMS motion sensor - 3-axis +-2g analog output "piccolo" accelerometer", STMicroelectronics Datasheet - LIS302SG, rev. 1, 2008

[5] D. E. Serrano, "Design and analysis of MEMS accelerometers", IEEE Sensors 2013, Tutorials, Conference, 2013

[6] STMICROELECTRONICS LSM303DLHC Series 3 Axis +-2/+-4/+-8/+-16 g 3.6 V Digital Accelerometer - VFLGA-14 - See more at: http://www.futureelectronics.com/en/technologies/semiconductors/analog LSM303DLHC.aspx?IM=0#sthash.Uds3FVRb.dpuf, visited 2015-02-05

[7] M. Lenkin and B. E. Boser, "A Three-Axis Micromachined Accelerometer with a CMOS Position-Sense Interface and Digital Offset-Trim Electronics", *IEEE Journal of solid-state circuits*, vol. 34, no. 4, pp. 456-468, 1999

[8] C. C. Tsang, "Error reduction techniques for a MEMS accelerometer-based digital input device", thesis in partial fulfillement of the requirements for a Ph.D., The Chinese Univeristy of Hong Kong, 2008

[9] I. Svensson, G. Wihlborg, "Mekanik i verkligheten", Lunds universitet, rev. 3, pp. 139-141, 2007

[10] D. Sjöberg, M.Gustafsson, "Kretsteori, ellära och elektronik", Lunds universitet, rev 4., pp. 77, 2011

[11] "Accelerometer Errors", Kionix application note - AN 012, 2007

[12] B. V. Amini, F. Ayazi, "Micro-gravity capacitive silicon-on-insulator accelerometers",*J. Micromech. Microeng.*, vol. 15, pp. 2113-2120, 2005

[13] "Ultra-compact high-performance eCompass module: 3D accelerometer and 3D magnetometer", STMicroelectronics Datasheet - LSM303DLHC, rev. 2, 2013

[14] J. Yang, J. B. Li, G. Lin, "A simple approach to integration of acceleration data for dynamic soil-structure interaction analysis", *Soil Dynamics and Earthquake Engineering*, vol. 26, pp. 725-734, 2006

[15] J. Yang, W. Chang, W.-C. Bang, E.-S. Choi, K.-H. Kang, S.-J. Cho, D.-Y. Kim, "Analysis and compensation of errors in the input device based on inertial sensors", *Proceedings of the international conference on information technology: coding and computing (ITCC'04)*, 2004

[16] STMicroelectronics MEMS Magnetometer Overview - Product Training Module, Digi-Key Corporation, http://dkc1.digikey.com/mx/en/tod/STMicroelectronics/MEMS-Magnetometer_NoAudio/MEMS-MagnetometerMagnetometer_NoAudio.ht visited 2015-02-06

[17] J. E. Lenz, "A review of magnetic sensors", *Proceedings of the IEEE*, vol. 78, no. 6, pp. 973-989, 2002

[18] V.Y. Skvortzov, H.-K. Lee, S.W. Bang, Y.B. Lee, "Application of electronic compass for mobile robot in an indoor environment", *Robotics and Automation, 2007 IEEE International Conference on*, pp. 2963-2970, 2007

[19] J.F. Vasconcelos, G. Elkaim, C.Silvestre, P. Oliveira, B. Cardeira, "A geometric approach to strapdown magnetometer calibration in sensor frame", *Aerospace and Electronic systems, IEEE Transactions on*, vol. 47, no. 2, pp. 1293-1306, 2011

[20] T. Ozyagcilar, "Layout recommendations for PCBs using a magnetometer sensor", Freescale Semiconductor Application note - AN4247, rev. 3, 2013

[21] "Using LSM303DLH for a tilt compensated electronic compass", STMicroelectronics Application note - AN3192, rev. 1, 2010

[22] Course notes on Magnetic materials from Boston university, http://physics.bu.edu/ duffy/PY106/MagMaterials.html, visited 2015-02-19

[23] US/UK World Magnetic Model - Epoch 2015.0, Main Field Total Intensity (F), developped by NOAA/NGDC and CIRES, http://www.ngdc.noaa.gov/geomag/WMM/data/WMM2015/WMM2015_ visited 2014-12-16

[24] T. Ozyagcilar, "Calibrating an eCompass in the presence of hard and soft-iron interference", Freescale Semiconductor Application note - AN4246, rev. 3, 2013

[25] K. A. Rahim, "Heading drift mitigation for low-cost inertial pedestrian navigation", Thesis submitted to the university of Nottingham for the degree of doctor of philosophy, 2012

[26] D. Vandermeulen, C. Vercauteren, M. Weyn, "Indoor localization using a magnetic flux density map of a building", *AMBIENT 2013: The Third International Conference on Ambient Computing, Applications, Services and Technologies*

[27] T. Ozyagcilar, "Implementing a tilt-compensated eCompass using accelerometer and magnetometer sensors", Freescale Semiconductor Application note - AN4248, rev. 3, 2012

[28] S. Nasiri, "A critical review of MEMS gyroscopes technology and commercialization status", InvenSense

[29] "Coriolis effect", *National geographic, encyclopedic entry*, http://education.nationalgeographic.com/education/encyclopedia/coriolis-effect/?ar_a=1, visited 2015-02-18

[30] STMICROELECTRONICS L3GD Series 2.4 - 3.6 V Three-axis Angular Rate Sensor - LGA-16. - See more at: http://www.futureelectronics.com/en/technologies/semiconductors/analog assemblies/Pages/7018358-L3GD20.aspx?IM=0#sthash.A3qVbltm.dpuf, visited 2015-02-05

[31] W.-C. Bang, W. Chang, K.-H. Kang, E.-S. Choi, A. Potanin and D.-Y. Kim, "Self-contained spatial input device for wearable computers", Proceedings on the Seventh IEEE International Symposium on Wearable Computers (ISWC'03), pp. 26-34, 2003

[32] C. Konvalin, "Motion/Velocity/Displacement Compensating for Tilt, Hard-Iron and Soft-Iron Effects", *sensors online*, 2009, http://www.sensorsmag.com/sensors/motion-velocity-displacement/compensating-tilt-hard-iron-and-soft-iron-effects-6475, visited 2015-03-12

[33] C. J. Fisher, "Using an accelerometer for inclination sensing", Analog Devices Application note - AN-1057, Rev. 0, 2010

[34] Moving average filtering - (a gentle introduction to noise filtering), Newcastle university, http://lorien.ncl.ac.uk/ming/filter/filmav.htm, visited 2015-03-12

[35] S. Sridhar, P. Rajesh Kumar, K. V. Ramanaiah, "Wavelet transformation techniques for image compression - an evaluation", *I. J. Image, Graphics and Signal Processing*, 2, pp. 54-67, 2014

[36] B. Vidakovic, P. Mueller, "Wavelets for kids - A tutorial introduction", Duke University, gt-wavelet.bme.gatech.edu/wp/kidsA.pdf, visited 2015-02-18

[37] Olbjer, L. "Experimentell och industriell statistik", Lunds tekniska högskola, Lunds universitet, rev. 5, pp. 55, 2000

[38] "Discovery kit for STM32F401 line", STMicroelectronics User manual - UM1669, rev. 1, 2013